



A review of cretaceous smooth-slopes extensional basins along the Iberia-Eurasia plate boundary: How pre-rift salt controls the modes of continental rifting and mantle exhumation

Yves Lagabriele, Riccardo Asti, Thibault Duretz, Camille Clerc, Serge Fourcade, Antonio Teixell, P. Labaume, Benjamin Corre, Nicolas Saspiturry

► To cite this version:

Yves Lagabriele, Riccardo Asti, Thibault Duretz, Camille Clerc, Serge Fourcade, et al.. A review of cretaceous smooth-slopes extensional basins along the Iberia-Eurasia plate boundary: How pre-rift salt controls the modes of continental rifting and mantle exhumation. Earth-Science Reviews, 2020, 201, pp.103071. <10.1016/j.earscirev.2019.103071>. <insu-02429025>

HAL Id: insu-02429025

<https://insu.hal.science/insu-02429025v1>

Submitted on 7 Jan 2021

HAL is a multi-disciplinary open access archive for the deposit and dissemination of scientific research documents, whether they are published or not. The documents may come from teaching and research institutions in France or abroad, or from public or private research centers.

L'archive ouverte pluridisciplinaire **HAL**, est destinée au dépôt et à la diffusion de documents scientifiques de niveau recherche, publiés ou non, émanant des établissements d'enseignement et de recherche français ou étrangers, des laboratoires publics ou privés.



HAL Authorization

A review of Cretaceous smooth-slopes extensional basins along the Iberia-Eurasia plate boundary: how pre-rift salt controls the modes of continental rifting and mantle exhumation

by :

Yves Lagabriele¹, Riccardo Asti¹, Thibault Duretz¹, Camille Clerc², Serge Fourcade¹, Antonio Teixell⁴, Pierre Labaume³, Benjamin Corre¹, Nicolas Saspiturry⁵

Addresses

1. Université de Rennes, CNRS, UMR 6118 Géosciences Rennes, Campus de Beaulieu, 35000 Rennes, France

2. ISEA, Université de la Nouvelle Calédonie, 98800 Nouméa, Nouvelle Calédonie

3. Géosciences Montpellier, CNRS-Université de Montpellier-Université des Antilles, 34095 Montpellier, France

4. Dept. de Geologia, Universitat Autònoma de Barcelona, 08193 Bellaterra, Spain

5. EA4592 Géoressources & Environnement, Bordeaux INP, Université Bordeaux Montaigne, 1 Allée Daguin, 33607 Pessac, France

Riccardo Asti riccardo.asti@univ-rennes1.fr, Duretz Thibault thibault.duretz@univ-rennes1.fr, Camille Clerc camille.clerc@univ-nc.nc, "Serge Fourcade; sg.fourcade@orange.fr" sg.fourcade@orange.fr, Antonio Teixell antonio.teixell@uab.cat, "Pierre Labaume" labauume@gm.univ-montp2.fr, "Benjamin Corre" benjcorre@hotmail.fr, Saspiturry Nicolas saspiturry.nicolas@gmail.com,

Corresponding author: Yves Lagabriele. yves.lagabriele@univ-rennes1.fr

Key words : Smooth-slopes basins; symmetrical profile; Iberia; Eurasia; Triassic evaporites; décollement layer; thermal anomaly; sedimentary burial; dominating-ductile tectonic regime.

Short abstract (for submission)

We enhance a striking correlation between the paleogeography of Upper Triassic deposits and the mode of crustal stretching of the north Iberia plate during the Cretaceous transtensional event. The basins which opened during the mid-Cretaceous times along the Iberia-Eurasia plate boundary (like the emblematic Parentis basin) exhibit a peculiar synclinal-shaped profile and are devoid of prominent block faulting. The top of the basement is characterized by gentle slopes dipping symmetrically towards the basin center. Based on a comparison with rifting models established from the North Pyrenean Zone, this architecture appear to result from the thinning of the central basin continental crust under dominating-ductile deformation in greenschist facies conditions. The common character shared by all the pre-rift sequences of the studied basins is the presence of a thick low-strength Upper Triassic evaporites and clays layer belonging to the Keuper group and forming a thick pre-rift low-strength unit. Efficient décollement along this layer triggers mechanical decoupling and gliding of the pre-rift cover remaining in the basin center as the continental crust is laterally extracted. Using recent paleogeographic reconstructions, we show that the distribution of the Keuper sediments remarkably matches the distribution of the Pyrenean and peri-Pyrenean, Parentis-type basins. This allows for the first time to propose a genetic link between the distribution of evaporite-bearing pre-rift sedimentary formations and the development of smooth-slopes rift basins.

56

57

Abstract

59

This article enhances for the first time a striking correlation between the paleogeography of Upper Triassic deposits and the mode of crustal stretching around and inside the Iberia plate during the Cretaceous transtensional event. In a first step, we propose a review of the architecture of the basins which opened during the mid-Cretaceous times along the Iberia-Eurasia plate boundary. Like the emblematic Parentis basin, all these basins exhibit a peculiar synclinal-shaped profile and are devoid of prominent block faulting. The top of the basement is characterized by gentle slopes, which dip symmetrically towards the center of the basins. Based on a comparison with recent geologically-based rifting models established from the North Pyrenean Zone, we propose that this architecture results from the thinning of the central basin continental crust under dominating-ductile deformation in greenschist facies conditions. The common character shared by all the pre-rift sequences of the studied basins is the presence of a thick low-strength Upper Triassic evaporites and clays layer belonging to the Keuper group and forming a specific pre-rift salt unit. In the studied basins,

73 efficient décollement along the Keuper evaporites and clays triggers mechanical decoupling
74 and gliding of the pre-rift cover that remains in the center of the basin as the continental
75 crust is laterally extracted. Thus, during the early rifting phase, the basement undergoes
76 thinning while the pre-rift cover remains preserved in the basin center. In response to hyper-
77 thinning and horizontal extraction of the continental crust, hot mantle material approaches
78 the detached pre-rift cover. The major consequences of this central basin thermal anomaly
79 are twofolds: (i) the ductile deformation of the thinned continental crust beneath the
80 detached pre-rift units, and (ii) the development of HT-LP metamorphic conditions in the
81 pre-rift sediments and at the base of the syn-rift flysch levels. This thermal event is well
82 recorded in the axial portion of the Pyrenean realm (future North Pyrenean Zone) as well as
83 in the pre-rift sediments of the Cameros basin (northern Spain). Continental stretching is
84 accommodated by shearing in the bulk upper and middle crust leading to the formation of
85 thin tectonic lenses of mylonitic crustal material remaining welded on the exhuming mantle.
86 The architecture of the smooth-slopes, Parentis-type basins studied in this article thus
87 contrasts with the structure of the Iberia-Newfoundland Atlantic margins which are
88 characterized by (i) top-basement detachment faults accommodating crustal extension
89 through rotation and translation of undeformed basement blocks, and (ii) by the
90 individualization of continental extensional allochthons lying tectonically over exhumed
91 lower crust or mantle rocks. Finally, using recent paleogeographic reconstructions, we show
92 that the distribution of the Keuper evaporites and clays remarkably matches the distribution
93 of the Pyrenean and peri-Pyrenean, Parentis-type basins. This allows for the first time to
94 propose a genetic link between the distribution of evaporite-bearing pre-rift sedimentary
95 formations and the development of smooth-slopes rift basins.

97 Introduction

98

99 More than 30 years ago, important steps in our understanding of the mechanisms of
100 continental rifting were achieved through the acquisition and interpretation of ECORS
101 seismic reflection profiles (1983-1994) (Damotte et al., 1998). New images of crustal and
102 Moho geometries beneath stretched continental crusts were obtained, shading light on
103 important discrepancies between structural patterns at the base of rift systems. In
104 particular, ECORS profiles from the Rhine graben and the Parentis basin displayed
105 contrasting images of the thinned upper lithosphere. In the first case, the upper crust
106 appears clearly rifted and offset by stepping normal faults (Brun et al., 1991) whilst, despite
107 slight tectonic inversion, the second case exhibits a smooth basement top, with gentle
108 slopes dipping symmetrically towards the basin center (Bois et al., 1997). Because only few
109 cases of Parentis-type architecture were observed worldwide, little attention has been paid
110 to this symmetrical, smooth-slopes type of continental rift, which apparently lacks major
111 upper crustal faulting and block tilting. Rather, most of the current models of rift-related
112 crustal thinning generally point to the individualization of a series of tilted continental blocks
113 indicating that the upper crustal levels behave in a dominant brittle mode in the proximal (or
114 continentward) as well as in the distal (or oceanward) margin domains. In such models,
115 shallow detachment faults accommodate the upper crustal extension through the rotation
116 and the translation of undeformed basement blocks. In the distal margin, these blocks,
117 referred to as extensional allochthons, are covered by syn-rift and post-rift sediments and
118 may lie tectonically over exhumed lower levels, including subcontinental mantle (Reston et
119 al., 1995; Manatschal et al., 2001; Jammes et al., 2010c; Osmundsen and Peron-Pinvidic,
120 2018, and references therein).

121 Recent geological investigations in the northern units of the Pyrenean belt forming the
122 North Pyrenean Zone (NPZ) as well as in the Basque-Cantabrian basin (fig. 1) show that
123 Parentis-type basins of mid-Cretaceous age were distributed all along the boundary between
124 the northern Iberia and southern Eurasia plates, thus introducing doubts regarding the
125 ubiquitous character of Iberia-Newfoundland-type margins (Lagabriele et al., 2010 ; Clerc
126 and Lagabriele, 2014; Teixell et al., 2016; 2018; Asti et al., 2019). In this article, we first list
127 the main characteristics of these Parentis-type basins, based on the analysis of detailed
128 geological reconstructions from areas exposed all along the northern flank of the Pyrenean

129 belt. Then we review the distribution of such basins at the scale of the Iberia and Eurasia
130 plates. We finally discuss some of the key-factors controlling the evolution of smooth-slopes
131 basins and we evaluate how such information increases our understanding of the
132 mechanisms of continental rifting and passive margin formation.

133

134 **I. Symmetrical, smooth-slopes basins of the north Iberia margin: insights from the North** 135 **Pyrenean Zone (NPZ) and the Basque-Cantabrian range**

136

137 The Pyrenees and the Cantabrian mountain (fig. 1) form a narrow, N110 trending fold-and-
138 thrust belt resulting from the collision of the northern edge of the Iberia plate (north Iberia
139 margin) with the southern edge of the Eurasia plate during the Late Cretaceous-Tertiary
140 (Choukroune and ECORS team, 1989; Muñoz, 1992; Deramond et al., 1993; Roure and
141 Choukroune, 1998; Teixell, 1998; Vergés and Garcia-Senz, 2001; Pedrera et al., 2017; Teixell
142 et al., 2018). Convergence initiated ca. 83 Ma, following an almost 40 Ma long period of
143 transtensional motion in relation with the counterclockwise rotation of Iberia relative to
144 Eurasia, also leading to oceanic spreading in the Bay of Biscaye between Chron M0 and A33o
145 (ca. 125-83 Ma) (Le Pichon et al., 1971; Choukroune and Mattauer, 1978; Olivet, 1996;
146 Sibuet et al., 2004). Convergence led to the partial or complete tectonic inversion of
147 discontinuous Cretaceous rift basins opened along the Iberia-Eurasia plate boundary during
148 the transtensional episode (Puigdefàbregas and Souquet, 1986; Debroas, 1990). Rotation
149 was achieved just before the Albian according to paleomagnetic data collected onland (Gong
150 et al., 2008). Earlier Triassic and Jurassic rifting events preceded the development of the
151 Cretaceous rifts (Canérot, 2017, and references therein).

152 Along the northern flank of the Pyrenees, more than forty, up to km-sized exposures of
153 subcontinental lherzolites are widespread within the Mesozoic pre-rift and syn-rift
154 sediments forming the NPZ (Monchoux, 1970; Vielzeuf and Kornprobst, 1984; Fabriès *et al.*,
155 1991, 1998). The NPZ is bounded by two major post-metamorphic thrusts, the North
156 Pyrenean Fault (NPF) to the South and the North Pyrenean Frontal Thrust (NPFT) to the
157 North. The NPF represents the tectonic boundary between the NPZ and the prominent axial
158 zone of the belt (AZ) constituted of a stack of Paleozoic basement units (Choukroune, 1976a;
159 1976b; 1978b).

160 Based on field and geophysical evidence from the central and western NPZ, exhumation of

161 sub-continental mantle is shown to have occurred coevaly with extreme thinning of the
162 continental crust in the Pyrenean realm during the mid-Cretaceous (Lagabriele and
163 Bodinier, 2008; Jammes et al., 2009; Masini et al., 2014). Therefore, mantle exhumation
164 (locally followed by peridotite exposure up to the floor of the Pyrenean basins) is now
165 considered as a general mechanism accounting for the presence of ultramafic material
166 within the NPZ. It is established that the well-known regional high temperature and low
167 pressure (HT-LP) Pyrenean metamorphism (Ravier, 1957; Azambre & Rossy, 1976; Bernus-
168 Maury, 1984) developed along the southern NPZ in relation with continental thinning during
169 the major Cretaceous extensional event (Vielzeuf and Kornprobst, 1984; Dauteuil and Ricou,
170 1989; Golberg & Leyreloup 1990; Clerc et al., 2015b; 2016). Following the early ECORS
171 profiles (Choukroune and ECORS team, 1989), additional information on the architecture of
172 the paleo-margin of Northern Iberia in the Pyrenees is provided by recent interpretation of
173 tomographic data acquired during the temporary PYROPE and IBERARRAY experiments
174 across the Pyrenees (Chevrot et al., 2015; 2018; fig. 1). Based on such data set, Wang et al.
175 (2016) suggest the inversion of a northern Iberia margin characterized by a short necking
176 domain and a large distal domain made of strongly attenuated crust (less than 10 km thick)
177 overlying a large volume of subcontinental mantle. As discussed further in this article, this
178 domain can be compared to large sheets of hyper-extended continental crust found in the
179 distal portions of present-day passive continental margins (see section III C)

180

181 Various models of continental crust thinning and associated mantle exhumation have been
182 proposed recently to account for geological constraints collected inside the metamorphic
183 NPZ. In figure 2 (profiles a to e), we present a selection of reconstructions extracted from
184 recent literature, which highlights numerous similarities between recently published models
185 of Cretaceous NPZ basins structure (Lagabriele et al., 2010; Clerc and Lagabriele, 2014;
186 Masini et al., 2014; Tugend et al., 2014; 2015; Clerc et al., 2016; Teixell et al., 2016, 2018;
187 Corre et al., 2016; Lagabriele et al., 2016; DeFelipe et al., 2017; Pedrera et al., 2017; Espurt
188 et al., 2019; Saspiturry et al., 2019; Asti et al., 2019; Ducoux et al., in review). Most of these
189 architecture models stress the role played by a major cover décollement layer during the
190 Cretaceous crustal thinning. This weak layer corresponds to the Upper Triassic Keuper
191 evaporites which contain clays and sands as well as minor carbonates and doleritic MORB
192 basalts (ophites). Its maximum thickness in the Pyrenean realm reached 2.7 km, as deduced

193 from field data in the southern Pyrenees coupled to well data in the Mauléon and Aquitaine
194 basins and the Bay of Biscay region (James & Canérot, 1988; McClay et al., 2004; Biteau et
195 al., 2006; Jammes et al., 2010a; 2010b; 2010c; Roca et al., 2011; Saura et al., 2016; Orti et
196 al., 2017; Saspiturry et al., 2019). In the décollement layer now exposed in the metamorphic
197 NPZ, the Triassic clays were transformed into talc and chlorite, and the carbonates most
198 often suffered intense tectonic brecciation with talc, tremolite and dolomite
199 recrystallizations (Thiébaud et al., 1992; Lagabrielle et al., 2019a, 2019b). Pre-rift to syn-rift
200 salt diapirism was also frequently observed in the non-metamorphic NPZ and in the
201 Southern Pyrenees (e.g. Canérot, 1988; 1989; Lenoble and Canérot, 1992; Canérot and
202 Lenoble, 1989; 1993; James and Canérot, 1999; Canérot et al., 2005; Jammes et al., 2009;
203 Jammes et al., 2010a; 2010b; Roca et al., 2011; Saura et al., 2016; Teixell et al., 2016).

204

205 As early stated by Clerc and Lagabrielle, (2014), the main consequence of the presence of
206 the low-strength Keuper layer along the north Iberia margin is that during the Cretaceous
207 rifting, the pre-rift Mesozoic cover was efficiently decoupled from the Paleozoic basement
208 along the evaporites and thus remained on top of the stretched continental lithosphere in
209 the center of the basin. It must be noted that in the external parts of the Pyrenean rift, the
210 borders of the subsiding Cretaceous flysch basins remain at low temperature and display
211 classical faulted and tilted blocks (e.g. half-grabens of Quillan basin, Camarade basin,
212 Gensac-Bonrepos basin, western border of the Mauléon basin, edges of the Gran Rieu high
213 and Lacq basin) (Debroas, 1978; 1990; Biteau et al., 2006; Lagabrielle et al., 2010; Masini et
214 al., 2014; Grool et al., 2018; Espurt et al., 2019).

215

216 The Cinco Villas Paleozoic massif and the Le Danois Bank (fig. 1) respectively form the
217 eastern and western boundary of the Basque-Cantabrian basin which develops to the west
218 of the NPZ towards the northern Iberia Peninsula. It is filled by an up to 12.5 km thick
219 succession of Upper Jurassic-Cretaceous sediments with interlayered Aptian to Santonian
220 basic volcanic rocks (Azambre and Rossy, 1976; Rat et al., 1983; Rat, 1988; Castañares et al.,
221 2001; García-Mondéjar et al., 1996; 2004; Floquet, 2004) (fig. 2f-h). This basin was floored by
222 an extremely thinned lithosphere in its central parts (Biscay Synclinorium and Nappes des
223 Marbres) and was also affected by a Late Cretaceous thermal metamorphism (Golberg and
224 Leyreloup, 1990; Cuevas and Tubía, 1999; Pedrera et al., 2017). A peridotite outcrop close to

the Leiza fault shows that crustal thinning led to the exhumation of the upper mantle close to the floor of the basin (Mendia and Gil-Ibarguchi, 1991; deFelipe et al., 2017). The basin architecture deduced from field investigations in the eastern part of the Basque-Cantabrian basin (the “Nappe des Marbres” area) includes smooth-slopes margins with normal faults and tilted blocks restricted to the external domains (deFelipe et al., 2017; Pedrera et al., 2017; Ducoux et al., in review). These reconstructed geometries bear affinities with basin architectures deduced from geological observations in the NPZ (fig. 2f-h). Indeed, such architecture and the overall evolution deduced for this rift system implicate gliding of the pre-rift sequence over its basement during crustal extension with ductile crustal thinning in its central part in a way similar to models deduced from NPZ studies (e.g. Clerc and Lagabrielle, 2014; Corre et al., 2016; Teixell et al., 2016). The Leiza detachment system of deFelipe et al. (2017) (fig. 2g) corresponds to the basal décollement allowing pre-rift sequence allochthony. The presence of a high-density mantle body beneath the Basque-Cantabrian basin has been established on the basis of lithospheric-scale gravity inversion (Pedrera et al., 2017). The association of this exhumed mantle body with rift and post-rift structural geometries suggests the activation of a major south-dipping ramp-flat-ramp extensional detachment between Valanginian and early Cenomanian times with horizontal extension of ~48 km. Interpretation of geophysical data shows that low-strength Triassic Keuper evaporites and mudstones above the basement favor the decoupling of the cover with formation of minibasins, expulsion rollovers, and diapirs (Pedrera et al., 2017).

245

Finally, the presence of a thick pre-rift salt layer underlying the Mesozoic carbonates appears as an ubiquitous parameter to take into account when reconstructing the evolution of the Cantabrian-Pyrenean range. Recent models of rift development at the northern Iberia margin show that Triassic lithology controls the three intrinsic characteristics of the Pyrenean rifting which can be summarized as follows:

- i. Tectonic juxtaposition of exhumed peridotites and pre-rift sediments. This occurs when the lateral extraction of the thinned continental crust is completed. In response to plate separation, the stretched crust is removed horizontally from the center of the rift and decoupling of the pre-rift cover from its basement occurs along the Keuper décollement. As a consequence a tectonic contact is established between the decoupled pre-rift sediments and the uplifted sub-continental mantle rocks

(Clerc and Lagabriele, 2014) (fig. 2e). In some locations, due to subsequent complete removal of the pre-rift cover, mantle rocks may be in turn exposed to the seafloor as observed around the Lherz, Urdach and Bestiac Iherzolite bodies (Lagabriele et al. 2010; 2016; de Saint Blanquat et al., 2016).

ii. Crustal stretching under dominantly-ductile conditions. The geometry of the thinned crustal units in the distal domain of the rift margins does not correspond to a succession of triangular-shaped isolated undeformed blocks (extensional allochthons) as described along the Iberia-Newfoundland conjugate margins and along the reconstructed alpine paleomargins (Manatschal, 2001; Manatschal et al., 2001; 2006; Peron-Pinvidic and Manatschal, 2009; Mohn et al., 2010; 2012; 2015) (fig. 3). By contrast, it appears as an assemblage of very thin lenses of ductilely deformed pre-Mesozoic material, originating mainly from the middle crust, separated by anastomosing shear zones that developed in greenschist facies conditions at low pressure (e.g. Corre et al., 2016; Teixell et al., 2016; Asti et al., 2019; Espurt et al., 2019) (fig. 2b-d). This important feature occurs because stretching develops under the allochthonous pre-rift cover that maintains moderate temperature in the upper and middle crust. Microscopic study of crustal material welded on the Urdach Iherzolites demonstrates that the middle crust was extracted laterally from the rift axis and deformed ductilely at temperatures between 450°C and 350°C (Asti et al., 2019). Large strains in the greenschist facies are testified by strongly elongate quartz ribbons in ortho- and para-derived mylonites with bulging recrystallization and brittle fracturing of feldspar in cataclastic flows (fig. 4a-b).

iii. Dominantly ductile deformation of the pre-rift and syn-rift sediments under HT-LP conditions. All along the rifting phase, the decoupled pre-rift cover remains in the center of the rift where the rift-related rise of the isotherms is more pronounced and where it is progressively buried under thick flysch sequence deposits. Sedimentary burial first preserves heat acquired during early rifting stages and second trigger temperature increase in the pre-rift cover. As a result, the detached pre-rift cover locally undergoes drastic syn-metamorphic ductile thinning and boudinage during continental breakup (fig. 5a-d). Such peculiar mechanical behaviour is outlined in all published rifting models (i.e. base of Nappe des Marbres basins, Leiza detachment system, base of Mauléon and Châinons Béarnais basin infills, base of Baronnies and

Boucheville basins infill, fig. 2). Progressive rifting triggers the upward propagation of the brittle-ductile transition which may reach syn-rift sediments deposited at the early stage of the basin opening (Clerc et al., 2016). Brittle deformation dominated by cataclastic brecciation follows ductile shearing and flattening in sedimentary units accompanying final exposure of mantle rocks to the seafloor, as proposed from studies in the Lherz area (Lagabrielle et al., 2016). The ductile-brittle transition is frequently observed at the mesoscopic and microscopic scale with sets of normal faults offsetting the extensional HT foliation (fig. 5e-f, 5h). Finally, at the scale of the entire rift, extensional deformation in the lower margin is accompanied by tectonic denudation of the cover in the upper margin (Lagabrielle et al., 2010; Teixell et al., 2016, 2018).

To sum up, figure 6 presents the intrinsic characteristics of the Pyrenean rifting listed above, compiled along an idealized column of the NPZ lithologies with photographs illustrating the most emblematic deformed levels exposed along the NPZ.

II. A review of smooth-slopes basins around the Pyrenees and Cantabrian ranges

Seismic images of oceanic margins and intracontinental rifts in the close surroundings of the Pyrenees and Cantabrian ranges bear crucial information on the mode of crustal thinning along the northern Iberia margin and adjacent areas during the Cretaceous.

(1) Parentis basin (fig. 1 and 7a). First interpretations of the Parentis ECORS profile point to a symmetrical, syncline-shaped basin, with only few normal faults in the stretched crust, even in the proximal domain (Pinet et al., 1987; Bois et al., 1997). Beneath the Parentis basin fill, the crust is less than 10 km thick and decreases westward from 7 km (along the ECORS Bay of Biscay profile, fig. 1), to 6–5 km (along the MARCONI 3 profile, fig. 1) (Tomassino and Marillier, 1997; Gallart et al., 2004; Ruiz, 2007). More recently, Jammes et al. (2010a), proposed that the southern Parentis basin represents a lower plate sag basin floored by a top-basement detachment system with an asymmetrical mode of opening. These authors emphasize the presence of a thick pre-rift salt layer in the area undergoing extreme crustal thinning, forcing sub- and suprasalt layers to deform differently. Whatever the processes of

321 crustal thinning are favoured, both older and recent models of Parentis basin evolution
322 highlight three major features: (1) the occurrence of symmetrical smooth-slopes gently
323 dipping basinward; (2) the presence of a crust which thins regularly towards basin axis,
324 without discrete steeply dipping faults, and (3) the presence of a thick pre-rift salt layer
325 allowing décollement of the pre-rift cover from its basement (Jammes et al., 2010b, 2010c).

326 (2) South Bay of Biscay margin (fig. 1, fig. 7b-c). Both the northern and southern margins of
327 the Bay of Biscay have been explored seismically. North-south transects of the Armorican
328 margin (Norgasis profiles, fig. 1: Thinon et al., 2003; Tugend et al., 2014) reveal a short
329 necking domain that concentrates most of the crustal deformation. Crustal thickness
330 decreases from 35 km at the shelf break to less than 10 km at the foot of the slope. Steep
331 rise of mantle implies the disappearance of the lower crust beneath the slope. Based on
332 results of gravity inversion combined with seismic interpretations, Tugend et al. (2014) map
333 a continuous domain of exhumed mantle from the Armorican basin toward the
334 hyperthinned Parentis basin where minimum crustal thickness occurs (fig. 7a) (Pinet et al.,
335 1987, Bois et al., 1996, Jammes et al., 2010a). According to Roca et al. (2011), the Bay of
336 Biscay Abyssal Plain itself consists of a transitional zone formed by a thin (4–9 km) crust with
337 riders of Mesozoic pre-rift and syn-rift sediments and continental crustal rocks that are
338 extensionally detached over an exhumed sub-continental mantle with seismic velocities
339 comprised between 7.2 and 8 km/s. The distal domain of the Bay of Biscay Abyssal Plain
340 bounds to the north the North Iberian margin, an extended continental margin with
341 Cretaceous basins (e.g. the Asturian basin, up to 10 km thick, fig. 1) and basement highs as
342 the Le Danois Bank (Cadenas and Fernández Viejo, 2016; Teixell et al., 2018), where
343 granulites have been dredged (Capdevila et al., 1980; Fügenschuh et al., 2003) (fig. 1).

344 (3) North-eastern Iberia intra-crustal basins (Iberian Chain and Valencia trough) (fig 1 and fig.
345 7b-d). Helpful additional information regarding the thinning modes of the northern Iberia
346 crust can be obtained from seismic images of the Los Cameros, Maestrat and Columbrets
347 basins now partly inverted in the Iberian Chain (fig. 1). These basins result from the
348 distributed extension of the northern Iberia plate synchronously with the opening of the Bay
349 of Biscay-Pyrenees in the mid-Cretaceous (Verges and Garcia-Senz, 2001; Mas et al., 2011).
350 They represent a well-developed Mesozoic rift having similarities with the North Atlantic
351 margins (Salas and Casas, 1993; Salas et al., 2001). In their internal parts, reconstructed

Iberian Chain basin geometries point to simple troughs exhibiting gentle slopes devoid of marked fault stepping, suggesting the absence of tilted blocks and a smooth basement top (e.g. Guimerà et al., 1995; Casas-Sainz and Gil-Imaz, 1998; Omodeo et al., 2014). The Moho generally shows an arched outline with a regular shallowing toward the basin center where the crust is reduced to some kilometers only. The Triassic evaporites play an important role during the Albian rifting in the basins of northeast Iberia. This role was recently well illustrated by interpretation of seismic reflection profiles in the Valencia trough (Etheve et al., 2018) (fig. 7b). These profiles reveal the presence of a large Albian basin, the Columbrets basin (fig. 1), filled with up to 10 km thick Mesozoic sediments over a highly extended continental basement locally only 3.5 km thick. The pre-rift and syn-rift successions form a large-scale synclinal with thinned borders, in relation with displacement along local extensional detachments. Whole deformation results of interaction between the thick pre-rift Triassic salt layer and dominantly ductile crustal thinning (Etheve et al. 2018) leading to the development of an abnormally thin continental crust (Gallart et al., 1990; Dañobeitia et al., 1992; Ayala et al., 2015). In the Cameros basin (fig. 7c-d), the pre-rift cover is decoupled on Triassic evaporites and is smeared all over the stretched domain. No major offset of the top basement is attested by the syn-rift record (Casas-Sainz and Gil-Imaz, 1998; Casas-Sainz et al., 2000). A striking feature is that like in the NPZ, HT-LP metamorphism associated with crustal thinning is reported in the Cameros basin fill (Guiraud and Séguret, 1985; Goldberg et al., 1988; Rat et al., 2019).

III. Discussion

A. Smooth-slopes basins: symmetrical geometries versus asymmetrical tectonic regime

A common characteristic of the smooth-slopes basins described in this review is the lack of tilted crustal blocks and related stepping fault scarps in their central part, thus defining a dominant symmetrical smooth-slopes profile of the basement top (figs. 2 and 7). Based on field data from the NPZ, we have shown that stretching of the crustal basement occurs in a dominant ductile mode under greenschist facies conditions, since the central part of the basin remains overlain by a permanent cover of detached pre- and syn-rift sediments. An important question is now to determine whether such symmetrical shapes result from

383 symmetrical or asymmetrical stretching processes.

384

385 The symmetry or asymmetry of the processes of lithosphere stretching and continental
386 breakup has been largely debated over the last 30 years (i.e. Buck et al., 1988; Allemand et
387 al., 1989; Buck, 1991; Brun, 1999, with references therein). More recently, the symmetrical
388 character of the final architecture of passive margins has been discussed by many authors
389 (i.e. Michon and Merle, 2003; Huisman and Beaumont, 2007; Reston et al., 1995; Sutra et
390 al., 2013; Brune et al., 2014). Apparent symmetry does not imply dominant pure shear
391 thinning mechanisms but may result from asymmetrical tectonic processes involving large-
392 scale discrete extensional shear zones (simple shear) as discussed by Nagel and Buck (2004)
393 (fig. 8a).

394

395 It is well admitted that architecture of extended crustal systems depends on the geometrical
396 and temporal associations between simple shear and pure shear regimes. In the pure shear
397 model of McKenzie (1978), designed to explain the evolution of sedimentary basins, the
398 lithosphere is stretched uniformly resulting in a symmetrical basin with faulting in the brittle
399 crust. By contrast, the simple shear model (Wernicke, 1981, 1985) points to one or few
400 detachment faults that originate at low-angle with dips less than 30° and concentrate the
401 entire deformation, so that, apart from the fault zones, the lithosphere is not deformed. The
402 simple shear model has been complicated with the adjonction of sequential detachments
403 faults (Lister and Davis, 1989). Combination of pure and simple shear model was further
404 proposed (Lister et al., 1991). In this combination model, crustal deformation is controlled
405 by low angle detachment faulting but thinning of the mantle lithosphere results from pure
406 shear. By introducing time-dependant rheological changes at the lithospheric scale, Reston
407 and Perez-Gussinye (2007) report a complex evolution from symmetric to asymmetric
408 extension, and back to symmetric, at margins displaying exhumed mantle in the hyper-
409 extended domain.

410

411 A laboratory model combining simple and pure shear has been realized by Brun and Beslier
412 (1996) in order to account for the exhumation of mantle rocks at ocean-continent
413 boundaries (fig. 8b). This model applies easily to the case of rifts with exhumed mantle such
414 as the Pyrenean and peri-Pyrenean smooth-slopes basins. This four-layer model is composed

415 of sand and silicone putty layers, regarded as analogues of the brittle and ductile layers of
416 both crust and mantle. However, it does not discriminate a mid-crustal level. The lower crust
417 deforms ductilely and the upper mantle is strong. Necking of the whole lithosphere model is
418 nearly symmetrical (pure shear) but asymmetrical structures (simple shear) develop
419 internally, due to boudinage and/or faulting of brittle layers. This model explains the
420 occurrence of shear zones in the mantle lithosphere as described by Vissers et al. (1995) in
421 the Pyrenean mantle and accounts for the ductile deformation of the crust as demonstrated
422 by Asti et al. (2019).

423

424 In contrast with the Brun and Beslier (1996) symmetrical model, recent models of margin
425 evolution based on the Iberian or Alpine examples have put forward asymmetric
426 architectures resulting from the development of few major detachment faults, and
427 promoted the use of “lower-” and “upper-plate” terminology (Manatschal, 2004; Mohn et
428 al., 2010, 2012, 2015; Sutra et al., 2013). Mohn et al. (2012) propose a model of three-layer
429 continental crust where the brittle upper and lower crusts are strongly decoupled by a
430 ductile middle crust (fig. 3b). Crustal thinning, accommodated through a so-called necking
431 zone, is the result of interplay between detachment faulting in the brittle layers and
432 decoupling in ductile quartzo-feldspatic mid-crustal levels along localized ductile
433 décollements. The excision of ductile mid-crustal layers and the progressive embrittlement
434 of the crust by coupling the lower and upper crusts enable major detachment faults to cut
435 into the underlying mantle, exhuming it to the seafloor.

436 In the Iberian and Alpine examples, authors envision the presence of one or few large-scale
437 discrete detachment faults controlling the entire crustal thinning and the basin subsidence.
438 This is also applied by Masini et al. (2014) in their model for the western NPZ where a major
439 north-dipping detachment fault accomodates the denudation of the sub-Eurasian mantle to
440 form the basement of the Mauléon basin (fig. 9a). Interpretation involving single
441 detachment faults has also been retained in the preliminary reconstructions of the NPZ
442 basins by Lagabriele and Bodinier (2008), Lagabriele et al. (2010) and Vauchez et al. (2013)
443 (fig. 9b, c), as well as in the reconstructed S-N transect from the Basque – Cantabrian to the
444 Armorican margin by Roca et al. (2011) (fig. 9d). Similarly, few detachment faults are used in
445 the Espurt et al. (2019), Saspiturry et al. (2019) and Ducoux et al. (in review) models for the
446 Barronies, Mauléon and “Nappe des Marbres” basins respectively (fig. 2). Others models

447 invoke deep-seated staircase extensional faults accounting for large-scale ramp-synclinal
448 folding as documented in the Cameros and Columbrets basins (Guimerà et al., 1995; Roma
449 et al., 2018). By contrast, models from the western NPZ by Corre et al. (2016) and Teixell et
450 al. (2016, 2018) (fig. 2) do not favor the activation of single detachment faults alone. Rather,
451 they involve symmetrical tectonic processes triggering a homogeneous thinning of the crust
452 during its lateral extraction from the rift axis.

453 In their study of the evolution of the western Betics including the exhumation of the Ronda
454 subcontinental mantle, Frasca et al. (2016) identify three successive steps: (i) ductile crust
455 thinning and ascent of subcontinental mantle thanks to mid-crustal shear zone and crust-
456 mantle shear zones acting synchronously; (ii) disappearance of the ductile crust bringing the
457 upper crust in contact with the subcontinental mantle, (iii) complete exhumation of the
458 mantle in the zone of localized stretching and high-angle normal faulting cutting through the
459 Moho, with related block tilting. These steps do not completely apply to the Pyrenean case,
460 notably because field and geophysical studies of the metamorphic NPZ never evidenced
461 brittle faulting of the Moho during the Cretaceous rifting.

462
463 Based on these examples of recent interpretations of rifting evolution, we stress that both
464 Alpine and Betic examples do not refer to a décollement level at the base of the pre-rift
465 cover. They promote evolutionary models lacking allochthony of the detached pre-rift
466 sediments, in contradiction with the examples detailed in section I and II. In addition, both
467 Alpine and Betic models refer to a progressive embrittlement in the rift axis resulting in the
468 complete elimination of ductile crustal layers. Again, this contrasts with the NPZ examples
469 where thin ductile crustal layers are extracted in the distal domain and remain welded on
470 the exhumed mantle.

471

472 **B. Smooth-slopes basins: crustal shear zones and lenticular fabrics at the mesoscale.**

473

474 Petrological studies of continental units exposed around the Urdach and Sarailé lherzolite
475 bodies (western NPZ) provide information on the deformation mode associated with crustal
476 thinning and mantle exhumation (Corre et al., 2016; Asti et al., 2019). Reconstruction of
477 sections across the NPZ Cretaceous basins by Clerc et al. (2015b), Teixell et al. (2016), Corre
478 et al. (2016) and Asti et al. (2019) use such ductile deformation mode having affinities with a

479 regional-scale, uniform pure shear mechanism. It is shown that extension in the Paleozoic
480 basement was achieved through lenticular deformation and pervasive ductile flattening with
481 anastomosing extensional mylonitic shear zones developing at temperatures of 350-450°C.
482 Here, during its lateral extraction from the rift axis, the crust thinned ductilely under
483 greenschist facies P-T conditions. Stretching occurred by the mean of undulating shear
484 contacts between tectonic lenses of flattened crustal material as described in figure 10. At
485 the final step of the continental breakup, very thin continental crustal lenses remained
486 welded on the exhumed mantle.

487 A very similar lenticular mode of deformation derives from investigations in the Basin and
488 Range province. Hamilton (1987) describes tectonic lenses of middle crustal rocks that
489 normally lie at separate levels in the crust with undulating shear contacts between them (fig.
490 8c). This deformation mode allows the juxtaposition of different lithologies by uplifting
491 deeper lenses during the extensional deformation. In a different way, Gartrell (1997)
492 propose a large scale crustal boudinage involving successive necking regions where the
493 ductile middle crust is extremely sheared (fig. 8d). The resulting architecture is a succession
494 of tectonic lenses that may evolve toward a large-scale lenticular geometry as proposed by
495 Espurt et al. (2019) for the evolution of the North Pyrenean massifs (fig. 2d).

496 In their recent detailed study of the tectonic and metamorphic evolution of the Urdach and
497 Sarailé mantle bodies and associated units, Lagabrielle et al. (2019a; 2019b) describe two
498 types of low-angle shear zones that accommodated part of extension of the distal domain of
499 the Iberia passive margin during the mid-Cretaceous (fig. 10a, b). The deepest shear zone is
500 the crust-mantle detachment. It separates the ultramafic mantle rocks from strongly thinned
501 continental Paleozoic rocks. It is composed of a basal 20-50 m thick lenticular layer of
502 sheared serpentinites followed by a 10 m thick damage zone. The lenticular layer consists of
503 ultramafic symmetrical tectonic lenses, a few meters long, separated by anastomosing
504 serpentine-rich shear zones. The damage zone consists of an assemblage of centimeter-sized
505 symmetrical lenses of a soft, talc-rich, sheared material, separated by conjugate shear zones.
506 The shallowest shear zone is the cover sole décollement. It corresponds to the tectonic
507 boundary separating the base of the detached pre-rift Mesozoic metasedimentary cover
508 from either mantle lherzolites or continental basement rocks. It consists of a thick
509 deformation zone (some meters to tens of meters thick) that was the locus of important
510 metasomatic crystallizations involving notably fluids of Triassic origin (Corre et al., 2016).

511 Detailed structural study of the basement and mantle rocks shows that it is not easy to
512 discriminate between dominant pure shear and dominant simple shear processes at the
513 outcrop and regional scales (Lagabrielle et al. 2019a; 2019b). Indeed, a major detachment
514 fault zone (typically related to regional simple shear) may contain abundant symmetrical
515 lenses suggesting locally dominant pure shear.

516 Finally, in the studied smooth-slopes basins, dominant pure shear mechanisms concentrate
517 into the strongly thinned continental tectonic lenses whereas simple shear mechanism
518 characterize the main detachments. Pure shear mechanisms associated with overall
519 flattening of the syn-rift and pre-rift sedimentary pile progressively develop into the basin
520 center as represented in figure 10a. Chronological constraints have to be integrated in order
521 to establish possible succession from simple shear-dominant toward pure shear-dominant
522 deformation mechanisms at the scale of the entire system.

523

524 **C. Smooth-slopes basins formation, insights for the evolution of passive, magma-poor** 525 **continental margins.**

526

527 We deduce from section B above that dominant pure shear deformation concentrates into
528 anastomosed tectonic lenses forming the strongly stretched continental in the central region
529 of smooth-slopes basins. In the following, we review examples of comparable uniform
530 modes of ductile deformation worldwide.

531 A lenticular mode of deformation devoid of any steep normal fault is proposed at the scale
532 of an entire passive margin by Gernigon et al., (2014) to account for the symmetrical
533 stretching of the continental crust during the formation of the Barents margin (fig. 11a). This
534 geometry recalls the structures proposed by Gartrell (1997) (fig. 8d). Lenticular fabric is also
535 suggested for deep crustal units connected to tilted blocks through listric faults along the
536 Norway margin (Osmundsen and Ebbing, 2008; fig. 11b). These structures accommodate
537 crustal thinning to only a few kilometer thicknesses through dominant ductile mode. The
538 symmetrical mode of stretching implying ductile thinning or boudinage of some crustal layer
539 can be compared to processes of depth-dependent stretching or thinning (DDT and DDS)
540 envisioned by Reston and McDermott (2014) in order to account for extensional
541 discrepancies at some passive margins. It must be noted that according to an interpretation
542 of deep seismic reflection profiles by Reston (1988), lens-shaped low-strain lozenges

543 separated by high strain shear zones form the structural pattern of the lower crust beneath
544 the United Kingdom. This overall pattern seems to be possibly applied to numerous units of
545 stretched crust at a large scale.

546 Several distal domains of North Atlantic passive margins display geometries that suggest the
547 presence of lens-shaped units of thinned to hyper-thinned continental crust detached along
548 anastomosing shear zones and now separated by large zones exposing exhumed mantle (e.g.
549 Labrador and West Greenland margins; Reston and Perez-Gussinyé, 2007) (fig. 11c, d). These
550 units do not resemble extensional allochthons of the West Iberia-type margins (figs. 2 and
551 11e) and show geometrical affinities with crustal boudins extracted during the Pyrenean
552 extension in the center of the Cretaceous rift (e.g. the Baronnies and Agly crustal boudins;
553 Espurt et al., 2019; Clerc et al., 2016) (fig. 2). Such large areas of hyper-thinned continental
554 crust possibly composed of an assemblage of heterogeneous boudins, can be viewed as
555 sheets representing considerable volumes of sheared and flattened continental material
556 (thickness less than 10 km, width of 100 km and length more than 1000 km, along the
557 margin), formed through processes of uniform pure shear at a crustal scale. We infer that
558 the modes of deformation exhibited by the Pyrenean crustal units welded on the exhumed
559 mantle (although at a much smaller scale) can apply to the formation of these crustal sheets,
560 suggesting predominance of greenschists facies mylonites. Similar crustal sheets underlying
561 sag basins are well imaged in recent numerical models of margin evolution (Brune et al.,
562 2014 ; Huisman and Beaumont, 2011; 2014) as shown in figure 12a, b. Crustal sheets are
563 present along the Angola margin (fig. 12d), they may be present in the very distal domain of
564 the Gulf of Lion margin where they may originate by extraction of lower crustal material
565 (Jolivet et al., 2017) (fig. 11f). Similar long and thin sheets are typically imaged by Wang et al.
566 (2016) at the base of the reconstructed Iberia margin of the Mauléon basin, and by Roca et
567 al. (2011) in their reconstruction of the north Iberia margin north of the Cantabrian coast
568 (fig. 9d).

569 In their compilation of high-quality and deep penetration seismic profiles of several passive
570 margins (Uruguay, Southern Namibia, Gabon, South China Sea and Barents Sea), Clerc et al.
571 (2015a; 2018) suggest that the lower crust of some margins is weaker than assumed and
572 accommodates a large part of extension by ductile shearing (fig. 8e). Boudinage appears as a
573 recurrent deformation process accounting for the thinning of the continental crust at
574 variable scales. This leads authors to an unorthodox vision of some type of passive margins

where: (i) the lower crust is weak, (ii) boudinage controls a large part of the deformation and localization of low-angle normal faults, and (iii) these normal faults often dip toward the continent. This study highlights a crustal behavior dominated by boudinage and lenticulation, implying interplay between ductile shear zones (boudin edges) and more resistant crustal volumes (boudin cores). As discussed above in section B, this deformation mode may apply to the thinned crustal levels in the axis of the Cretaceous Pyrenean rifts (Teixell et al. 2016, 2018; Asti et al., 2019) (fig. 10) and is supported by recent numerical models of lithospheric rifting incorporating macroscale anisotropy (Duretz et al., 2016). In their interpretation of deep seismic profiles of the Gulf of Lion margin, Jolivet et al. (2015) point to an intense stretching of the distal margin and reveal a 80 km-wide ocean-continent transition zone that may consist of thin lower continental crust (the “Gulf of Lion metamorphic core complex”) and exhumed mantle (fig. 11f). They infer an overall hot geodynamic environment with a shallow lithosphere-asthenosphere boundary able to weaken the upper mantle and the lower crust enough to make them flow south-eastward. In this example, the lower crust bears an important role, which is not fully documented by field data in the NPZ since evidence of exposure of lower crustal levels during the Cretaceous rifting event has not yet been reported with confidence. Moreover, in most of the sections of figures 3 and 7, the lower crust is considered as a high-strength layer that does not deform ductilely but tends to break into large scale boudins and to remain at depth during the rifting processes (e.g. figs. 2a, e, f, h).

595

596 **D. Comparison with thermo-mechanical models of crustal hyper-extension.**

597

The examples discussed above lead us to emphasize the frequency of lenticular fabrics at various scales reported from different studies in both the upper mantle and the crust. The formation of lenticular fabrics, necking and lateral extraction during continental rifting have been addressed in mechanical and thermo-mechanical numerical models (Duretz and Schmalholz, 2015; Duretz et al., 2016). These models emphasize the role of a pre-existing macroscopic mechanical anisotropy on the development of continental rifts. They illustrate the interplay between necking and lateral extraction of strong layers along weak décollements, thus defining a lenticular fabric and anastomosed shear zone networks at the regional scale as envisioned in the NPZ case.

Models of metamorphic core complexes (MCCs) formation generally involve a thick and hot continental crust (Brun and van den Driessche, 1994). This does not apply to the Pyrenean case but constructive inputs can be expected from a confrontation with the rheological parameters used for MCCs modeling. For instance, Tirel et al. (2008) use initial Moho temperatures of 800°C or higher, with crustal thicknesses of 45 km or greater. This is much more than what can be retained for the post-Variscan crust in the Pyrenees (thicknesses between 30 and 20 km) (Teixell et al., 2018, and references therein) and Moho temperatures lower than 800°C. In the Tirel et al. (2008) experiment, the exhumation process of the metamorphic dome results in the progressive development of a detachment zone and the Moho remains flat because the lower crust has a low viscosity and the upper mantle is weak enough. With Moho temperatures lower than 800°C, the sub-Moho mantle has high strength and effective viscosity resulting in strong Moho deflection and crustal-scale necking. These conditions (relatively cold mantle and thin crust) are reached in the Pyrenean rift explaining why the Pyrenean mantle rapidly reached the surface when it was passively mobilized in response to the drift of the Iberia plate.

A former numerical model that applies to the formation of passive continental margins suggests that the crust may be thinned by permanent pure shear both at the proximal and distal margin (Huisman and Beaumont, 2011) (fig. 12a). This scenario can apply easily to the Pyrenean case where the ductile behaviour of the middle crust is demonstrated (Asti et al., 2019). The Huisman and Beaumont (2011) model produces symmetric margins associated with distal domain characterized by large sheets of thinned crustal material, as discussed above. The symmetrical outline is well imaged by current reconstructions of the Pyrenean basins from the North Pyrenean Zone and associated examples (Parentis, Cameros and Columbrets basins, fig. 1, 2 and 7).

Brune et al. (2014) produce a different numerical model that emphasizes a rift migration accomplished by sequential upper crustal faults balanced through lower crustal flow (fig. 12b). An interesting concept is that of 'exhumation channel', a weak locus of deformation where the crust and part of the uppermost mantle are actively deformed and extremely thinned during their transfer from lower to shallower levels, over a dome of upwelling lithospheric mantle. This high strain volume is not a detachment fault and thus may bear some affinity with the lenses of crustal material exhumed with NPZ mantle and described by Asti et al. (2019). As discussed in section C above, the resulting geometry is that of areas of

639 drastically thinned crust (named *crustal sheets* in the following) forming the distal margin
640 domain lying over a cooled and strengthened mantle. This mantle is exposed locally at the
641 rift axis depending on the extension rate. The final sketch derived from this model, including
642 a dome of strong mantle rimmed in its upper part by a thin layer of mylonitic crust, is a
643 reliable image for the geometry resulting from the Pyrenean rifting and associated basins at
644 a lithospheric scale.

645 Jammes et al. (2015) and Jammes and Lavier (2016), introduced compositional complexities
646 in the lithosphere by using an explicit biminerale assemblage which results in the
647 development of anastomosing shear zone. In their models, the deformation appears
648 localized in the middle/lower crust and the upper lithospheric mantle and leads to the
649 preservation of almost undeformed lenses of material surrounded by localized shear zones
650 concentrating most of the deformation. Such a lenticular final geometry is also evocative of
651 the one observed in the North Pyrenean Zone as discussed in detail by Asti et al. (2019) and
652 illustrated in fig. 10.

653 To unravel the dynamic evolution of the Cretaceous Pyrenean rift, Duretz et al. (2019)
654 carried out a set of thermo-mechanical numerical models of lithosphere-scale extension
655 based on the available geological constraints listed above in section I. The models were used
656 to explore the role of a km-thick basement-cover décollement layer at the base of the pre-
657 rift sediments. These numerical experiments highlight the key-role of the décollement layer
658 that can alone explain collectively: (i) salt tectonics deformation style and cover
659 décollement, (ii) high temperature metamorphism of the pre-rift cover, and (iii) ductile
660 mode of crustal thinning in the inner domain of the models. In the axis of the synclinal-
661 shaped basin ("sag" basin in the margin literature), extreme pure shear leads to the
662 development of a very thin basement layer, overlain by poorly-thinned pre-rift and syn-rift
663 sediments and underlain by exhuming mantle. These models are in good agreement with the
664 current knowledge of the architecture of the Cretaceous Pyrenean basins as exemplified by
665 reconstructions of figs. 2 and 7, as well as with the presence of large sheets of hyper thinned
666 crustal material (crustal sheets) in the distal part of numerous magma poor passive margins.

667

1261
1262
1263 **668 E. The pre-rift salt décollement layer: a mechanical key-factor in the evolution of smooth-**
1264
1265 **669 slopes basins. Establishing a new link between Triassic paleogeography and rifting**
1266
1267 **670 mechanisms.**

1268
1269 671

1270 672 As reported in section I and II, the common character between all pre-rift sequences of the
1271
1272 673 aforementioned smooth-slopes basins is the presence of the thick low-strength Late Triassic
1273
1274 674 evaporitic layer (Keuper). All related geological and geophysical studies highlight the
1275
1276 675 importance of this décollement layer in the evolution of the rift basins under study. As
1277
1278 676 detailed above, efficient décollement along the Keuper evaporites and clays triggers
1279
1280 677 mechanical decoupling and gliding of the pre-rift cover that remains in the center of the
1281
1282 678 basin as the crust is laterally extracted. In response to crustal hyper-thinning and horizontal
1283
1284 679 crustal extraction, hot mantle material approaches the detached pre-rift cover. As a
1285
1286 680 consequence, HT-LP metamorphism develops in the pre-rift sediments and at the base of
1287
1288 681 the syn-rift flysch levels as recorded in the NPZ and in the pre-rift sediments of the Cameros
1289
1290 682 basin. Subsequent deposition of syn-rift sediments allows preservation of the initial thermal
1291
1292 683 anomaly with a major consequence on the deformation regime in the pre-rift sediments and
1293
1294 684 crustal basement. Temperature increase in the NPZ basins center progressively leads to the
1295
1296 685 uprise of the brittle/ductile transition avoiding the development of prominent crustal normal
1297
1298 686 faults and leading to the dominantly ductile thinning of the Paleozoic basement and parts of
1299
1300 687 the pre-rift and syn-rift sediments (Clerc and Lagabriele, 2014; Clerc et al., 2015b; Asti et al.,
1301
1302 688 2019; Duretz et al., 2019). We may now question the paleogeographic distribution of the
1303
1304 689 Keuper group sediments at the Europa-Iberia scale in order to evaluate a possible link
1305
1306 690 between modes of rift development and the occurrence of a thick Keuper layer at the base
1307
1308 691 of the pre-rift sequence.

1309 692 Several extensional systems interacted in the Iberia platform during the Trias, resulting in
1310
1311 693 the creation of intraplate basins or troughs including the Valencian, Basque-Cantabrian, and
1312
1313 694 Pyrenean basins (figs. 1 and 13). The sedimentary infill of these platform basins continued
1314
1315 695 throughout the Mesozoic. Seismic, well and field data from the Bay of Biscay region, the
1316
1317 696 Pyrenees and the Aquitanian Basin, suggest initial thickness of Upper Triassic formations
1318
1319 697 ranging from 1000 to 2700 m (James and Canérot, 1999; Biteau et al., 2006; Jammes et al.,
1320
698 2010a; Roca et al., 2011; Rowan, 2014; Lopez-Mir et al., 2014; Saura et al., 2016; Soto et al.,
699 2017; Zamora et al., 2017). The salt-rich layers generally consist of shales and evaporites

700 including dominant gypsum and minor halite and anhydrite (figs. 13 and 14).
701 Paleogeographic reconstructions are available for the Triassic period at the scale of the
702 Iberia-western Europa region (Dercourt et al., 1986; 1993; Ziegler, 1988; Ortí et al., 2017;
703 Soto et al., 2017). The distribution of Triassic shales and evaporites is contrasted around the
704 future Iberia plate margins. This paleogeography is confirmed by a compilation of data
705 collected independantly by D. Frizon de Lamotte (fig. 13c). Evaporites are well developed
706 along the eastern edge of Iberia (Tethys side) and in the rift opened at the place of the
707 future NPZ, the Basque-Cantabrian basin, the Bay of Biscaye basin and the southern part of
708 the Armorican margin. In the place of the future North Atlantic rift system, evaporites are
709 restricted to the Peniche, Lusitanian, Alentejo and Algarve basins along the southern half of
710 the Portugal margin and are lacking along the northern half of the Iberia Atlantic margin.
711 Along the conjugate north American margin, evaporites are known at the base of the
712 Jeanne-d'Arc basin and are of restricted extension compared to the Keuper group exposed in
713 Central Europe (fig. 13b, c).
714 Finally, along the western half of the Iberia-Newfoundland transect, evaporitic formation are
715 not reported, whereas thick evaporites are reported from areas characterized by Parentis-
716 type basins. As outlined in figures 13 and 14, this paleogeography matches the distribution
717 of the two opposite types of basins discussed in this article (Parentis type vs. Iberia-
718 Newfoundland type). Thus, we establish a link between the presence of a pre-rift salt layer
719 and the deep mechanisms of crustal stretching. Because they remain in the center of the
720 basin, evaporites contribute to the preservation of a rather high thermal gradient in the axial
721 rift allowing a dominant-ductile deformation of the basement. The lack of a major
722 décollement level at the base of the pre-rift sequence may explain by itself why pre-rift
723 sediments remain welded and coupled to the basement on the top of tilted blocks in the
724 Iberia-Newfoundland-type margins as illustrated in figure 3a, b. Indeed, in the Iberia as well as
725 in Alpine margin-types, only syn-rift sediments are deposited over the exhumed lower
726 crustal levels and subcontinental mantle (Péron-Pinvidic et al., 2007; Péron-Pinvidic and
727 Manatschal, 2009; Mohn et al., 2012), which contrasts with the evolution of the Parentis-
728 type basins.

729

730 In this review, on the basis of examples clustering along the Iberia-Eurasia plates boudaries,
731 we emphasize the major role played by the Upper Triassic evaporitic layer during extensional

1381
1382
1383 732 processes. In the reported smooth-slopes basin examples, cover gliding occurred on a pre-
1384
1385 733 rift layer and thus contrasts with cases involving syn- to post-rift weak layers. The latter
1386
1387 734 cases have been largely documented by studies of passive margins displaying thick syn-rift
1388
1389 735 salt formations such as the Angola margin where the post-salt sedimentary units have glided
1390
1391 736 gravitationally after the margin formation (e.g. Brun and Fort, 2011, and references therein,
1392
1393 737 see also additionnal discussion relative to the pre-rift/post-rift salt effects during rifting in
1394
1395 738 Jammes et al., 2010c). To sum up, the specific characters emphasized in this review are
1396
1397 739 twofold : (i) the peri-Pyrenean salt is pre-rift allowing conservation of the pre-rift cover over
1398
1399 740 the high-strain axial rift. Crustal faulting has not disrupted the continuity of the Triassic
1400
1401 741 evaporite formation, allowing for décollement of the pre-rift sequence basinward, down to
1402
1403 742 the distal margin. (ii) Consequently, the axial thermal anomaly is preserved and the
1404
1405 743 dominant ductile mode of crustal deformation prevented the formation of faulting-related
1406
1407 744 steps leading to smooth-slopes basin edges.

1405
1406 745

1407 746 **F. Time-dependent rheology during the evolution of smooth-slopes basins**

1408
1409 747

1410 748 From the statements listed at the end of section I as well as from the discussion above, we
1411
1412 749 first stress that the models of Pyrenean Cretaceous rifting established on the basis of
1413
1414 750 geological constraints from the NPZ differ significantly from the classical models of passive
1415
1416 751 margin formation based on the Iberia-Newfoundland margins example (Peron-Pinvidic and
1417
1418 752 Manatschal, 2009; Sutra et al., 2013; Osmundsen and Peron-Pinvidic, 2018, and references
1419
1420 753 therein). The latter models involve a dominantly brittle behavior of the crust and the
1421
1422 754 individualization of tilted faulted blocks bearing a concordant pre-rift cover permanently
1423
1424 755 welded on their back (fig. 3). In the models based on the geology of the NPZ (e.g. models of
1425
1426 756 Clerc et al., 2016; Teixell et al., 2016; Espurt et al., 2019), the external borders of the
1427
1428 757 subsiding Cretaceous flysch basins remain at low temperature and display classical faulted
1429
1430 758 and tilted blocks (e.g. half-grabens of Quillan basin, Camarade basin, Gensac-Bonrepos
1431
1432 759 basin, western border of the Mauléon basin, Arbailles basin, edges of the Gran Rieu high and
1433
1434 760 Lacq basin). By contrast, in the internal regions of the rift system (corresponding to the
1435
1436 761 future metamorphic NPZ), the basement thinned in a dominant-ductile mode because
1437
1438 762 temperature conditions reached 350°C to 450°C beneath the detached pre-rift cover and the
1439
1440 763 syn-rift flysch.

1441
1442
1443 764 The peculiar evolution of the NPZ basins is depicted on figure 15 based on an original model
1444
1445 765 by Clerc et al., (2016). This model is strictly conceptual and was designed to account for
1446
1447 766 geological constraints gathered from various sites along the NPZ. The simplified system
1448
1449 767 includes the subcontinental mantle, a continental basement, a first decollement level in
1450
1451 768 Triassic evaporites, a level of layered pre-rift carbonates and a cover of syn-rift flysch. The
1452
1453 769 carbonates are able to deform by crystalline plasticity of calcite under HT conditions. The
1454
1455 770 corresponding lithologies are illustrated and briefly described in the NPZ lithostratigraphical
1456
1457 771 column of figure 5.

1458
1459 772 In order to better assess the time-dependent rheological changes that necessarily affect
1460
1461 773 each geological layer involved during this three steps evolution, we provide synthetic
1462
1463 774 rheological profiles and geotherms for selected parts of the basin: in the external portion
1464
1465 775 representing the initial pre-extension model (fig. 15a) and in the center of the basin for the
1466
1467 776 following two steps (fig. 15b and c). The data used to construct these profiles derived from
1468
1469 777 the Duretz et al. (2019) model discussed in section D above.

1470
1471 778 The three steps of this conceptual evolutionary model can be described as follows:

1472
1473 779 (1) At an early rifting stage (fig. 15a) moderate extension leads to crustal thinning
1474
1475 780 accommodated through normal faults in the upper crust. The rheological profile consists of a
1476
1477 781 15 km thick, cold and brittle upper crust ($T > 300^{\circ}\text{C}$) overlying a 15 km thick ductile lower
1478
1479 782 crust with Moho temperature around 550°C . The uppermost mantle is a strong 15 km thick
1480
1481 783 layer. In the inner part of the system, normal faults may pass downward to ductile shear
1482
1483 784 zones dipping toward the external side thus delineating a small central horst. The Triassic
1484
1485 785 evaporitic layers act as a décollement layer that allows the pre-rift carbonates to remain in
1486
1487 786 the most thinned and subsiding domains on both sides of the central horst while the syn-rift
1488
1489 787 flysch is being deposited above. Sliding of the pre-rift carbonates in the deep domain results
1490
1491 788 in the local tectonic denudation of the margins where carbonates remnants form isolated
1492
1493 789 rafts tilted on listric faults.

1494
1495 790 (2) At the mid-rifting stage (fig. 15b), ductile thinning of the crust occurs in response to
1496
1497 791 heating due to rapid mantle uplift. The central crustal horst starts to deform ductilely and
1498
1499 792 progressively acquires a lens shape. Due to blanketing effect under the syn-rift sediments,
1500
793 the HT pre-rift carbonates suffer syn-metamorphic ductile deformation. Rheological profile

794 in the center of the basin shows the Keuper weak zone at the base of the pre-rift cover and a
795 newly formed weak zone corresponding to the thinned crust which deforms at temperatures
796 between 300°C and 500°C. The lower crust has been extracted laterally and the brittle
797 mantle layer shows a decreasing thickness due to temperature increase from 400°C (step 1)
798 to 1000°C at only 20 km depth.

799 (3) At the final rifting stage (fig. 15c), extreme thinning and boudinage of the crust leads to
800 local denudation of the sub-continental mantle, which is by place in tectonic contact with
801 the pre- or syn-rift sediments. The crust in the center of the basin has been cut into few
802 lenses that move independently. The crust at both edges of the proximal domain thins and
803 moves horizontally (*lateral extraction* concept of Clerc and Lagabrielle, 2014). The Triassic
804 décollement layer undergoes drastic thickness reduction leading to boudinage in response
805 to fluid-assisted tectonic brecciation and to metasomatic dissolution as observed in the
806 Urdach and Sarailé massifs in the western NPZ (Lagabrielle et al., 2019a, 2019b in press).
807 Due to their increasing plasticity, the HT marbles of the pre-rift cover progressively
808 accommodate a large part of the deformation at the base of the basin, involving calcite
809 plasticity and recrystallization, boudinage, drag folding and low angle normal shear bands. In
810 turn, the lower levels of the syn-rift flysch sequence are progressively affected by HT
811 metamorphism and ductile deformation with bedding-parallel foliation and boudinage.
812 Continuous extension of the basin floor leads also to the progressive exhumation of the
813 metamorphic pre-rift sediments, which are progressively extracted from below the syn-rift
814 cover (see complete description of this process in Clerc et al., 2016). In the thinnest crustal
815 portion, the rheological profile bears similarities with that of step 2. The crustal thickness
816 has now reduced to less than one km and the brittle/ductile transition has moved upward.
817 The pre-rift cover, salt décollement as well as the thinned basement thus deform under
818 dominant ductile deformation.

819 IV. Conclusions

820

821 Almost fourty years after the discovery of mantle exhumed at the foot of the north Iberia
822 passive margin (Boillot et al. 1980), this review highlights the affinities between the
823 architecture of two types of extensional basins now variously inverted in the Pyrenean
824 orogeny. These are : (i) the extensional basins that opened during the mid-Cretaceous times

825 along the Iberia-Eurasia plate boundary and, (ii) the intraplate basins of northern Iberia
826 (Cameros to Columbrets basins). Taking as a reference the Parentis basin profile and on the
827 basis of geological reconstructions of NPZ rift architecture, we have designed an idealized
828 cross-section of a smooth-slopes basin shown in figure 16. The dominant features put
829 forward in this cross-section relate to the basin central region which lacks stepping normal
830 faults and large-scale tilted crustal blocks. The section shows a dominant symmetrical shape
831 with smooth-slopes that relates to a new mode of crustal stretching during continental
832 rifting characterized by a ductilely thinned crust in the central rift domain. This deformation
833 mode is typically symmetrical and contrasts drastically with stretching processes described
834 from the Iberia-Newfoundland and Alpine Tethys margins implying asymmetrical
835 architecture and extensional detachment separating upper and lower plates having
836 differential evolution.

837

838 The common character between all pre-rift sequences of the studied basins is the presence
839 of the thick low-strength Late Triassic evaporitic layer (Keuper facies). Geological and
840 geophysical studies point to the importance of this décollement layer in the evolution of
841 these rift basins. As established by geological studies in the NPZ, efficient décollement along
842 the Keuper evaporites and clays triggers mechanical decoupling and gliding of the pre-rift
843 cover that remains in the center of the basin as the crust is laterally extracted. Subsequent
844 deposition of syn-rift sediments allows preservation of the initial thermal anomaly with a
845 major consequence on the deformation regime in the pre-rift sediments and crustal
846 basement. The ubiquitous character of the ductilely deformed marbles in the metamorphic
847 NPZ relates to a dominant-ductile deformation regime in the pre-rift cover during the
848 Cretaceous extension. In these smooth-slopes basins, the ductilely stretched crust behaves
849 homogeneously at the regional scale and extensional allochthons are not individualized. A
850 lenticular mode of homogeneous deformation is thus defined implying interplay between
851 hectometric lenses of ductile crustal material separated by anastomosing shear zones.

852

853 Both laboratory and thermo-mechanical numerical models reproduce remarkably the mode
854 of deformation deduced from geophysical and geological constraints compiled in the studied
855 basins. Thus it appears that the pre-rift character of the salt layer is the key-factor of the

856 rifting style in controlling the very early decoupling between the basement and the pre-rift
857 cover. This strongly contrasts with the evolution of Atlantic margins where the salt is either
858 syn-rift or post-rift. For the first time, we evidence a strong link between the occurrence of a
859 sedimentary layer covering the future rifted region (here Keuper salt and clays deposits) and
860 a mode of crustal thinning (here homogeneous bulk ductile deformation). Décollement
861 along the evaporites and clays level finally favors the formation of symmetrical basins
862 lacking numerous normal faults and related tilted blocks. This new mode of crustal
863 deformation might not be restricted to the Pyrenean region, but may apply to all regions
864 hosting thick pre-rift décollement series. It may have been active worldwide, in the distal
865 portion of continental margins devoid of typical tilted blocks and extensional allochthons
866 and where large units of extremely thinned continental crust are present.

867

868 To sum up, the specific characters of the smooth-slopes basins emphasized in this review are
869 twofold: (i) the peri-Pyrenean salt is pre-rift allowing conservation of the pre-rift cover over
870 the high-strain axial central region. The continuity of the Triassic evaporite formation is
871 preserved allowing for décollement of the pre-rift sequence which remain in the basin
872 center. (ii) Consequently, the axial thermal anomaly is preserved and the dominant ductile
873 mode of crustal deformation prevents the formation of faulting-related steps, thus leading
874 to smooth-slopes basin edges. Continuous sedimentation in the subsiding basin leads to
875 progressive sedimentary burial of the prerift sequence. This in turn allows the preservation
876 of the initial thermal anomaly that may grow during the rifting evolution.

877

878 **Acknowledgements**

879 This work is the result of a 10 years field and laboratory research conducted in the Pyrenean
880 range with funding from various programs and institutions. We benefited of grants from the
881 French ANR Pyramid program, the Bureau de Recherche Géologique et Minière (BRGM),
882 Référentiel Géologique de la France (RGF) program and the Total/INSU/BRGM OROGEN
883 program with contributions from the CNRS and from Géosciences Montpellier and Rennes
884 research units. We thank Thierry Baudin (BRGM) and Sylvain Calassou (Total) for program
885 management and encouraging discussions. We also thank B. Azambre, P. Boulvais, M. Pujol,
886 and many others for stimulating exchanges that helped improve our ideas.

1681
1682
1683
1684
1685
1686
1687
1688
1689
1690
1691
1692
1693
1694
1695
1696
1697
1698
1699
1700
1701
1702
1703
1704
1705
1706
1707
1708
1709
1710
1711
1712
1713
1714
1715
1716
1717
1718
1719
1720
1721
1722
1723
1724
1725
1726
1727
1728
1729
1730
1731
1732
1733
1734
1735
1736
1737
1738
1739
1740

887

889 References

- 890
- 891 Allemand, P., Brun J.-P., Davy P., and Van Den Driessche J., 1989. Symétrie et asymétrie des
892 rifts et mécanismes d'amincissement de la lithosphère, *Bull. Soc. Géol. Fr.*, 5, 445–451.
- 893
- 894 Asti, R., Lagabrielle, Y., Fourcade, S., Corre, B., Monié, P., 2019. How do continents deform
895 during mantle exhumation? Insights from the northern Iberia inverted paleopassive margin,
896 western Pyrenees (France). *Tectonics*, 38, 1666–1693.
897 <https://doi.org/10.1029/2018TC005428>
- 898
- 899 Ayala, C., Torne, M., Roca, R., 2015. A review of the current knowledge of the crustal and
900 lithospheric structure of the Valencia Trough Basin. *Bol. Geológico Min.* 126, 533–552.
- 901
- 902 Azambre, B., Rossy, M., 1976. Le magmatisme alcalin d'âge crétacé, dans les Pyrénées
903 occidentales et l'Arc basque; ses relations avec le métamorphisme et la tectonique. *Bull.*
904 *Société Géologique Fr.* 7, 1725–1728.
- 905
- 906 Bernus-Maury, C., 1984. Etude des paragéneses caractéristiques du métamorphisme
907 mésozoïque dans la partie orientale des Pyrénées. Thèse, Pierre et Marie Curie, Paris.
- 908
- 909 Biteau, J.-J., Le Marrec, A., Le Vot, M., Masset, J.-M., 2006. The Aquitaine Basin. *Pet. Geosci.*
910 12, 247–273.
- 911
- 912 Boillot, G., S. Grimaud, A. Mauffret, D. Mougenot, J. Kornprobst, J. Mergoïl-Daniel, and G.
913 Torrent, 1980. Ocean-continent boundary off the Iberian margin: A serpentinite diapir west
914 of the Galicia bank, *Earth Planet. Sci. Lett.*, 48, 23–34.
- 915
- 916 Bois, C., Gabriel, O., Lefort, J.-P., Rolet, J., Brunet, M.-F., Masse, P., Olivet, J.-L., 1997.
917 Geologic contribution of the Bay of Biscay deep seismic survey: a summary of the main
918 scientific results, a discussion of the open questions and suggestions for further
919 investigation. *Mém Soc Géol Fr.* 193–309.
- 920
- 921 Brun, J. P., 1999. Narrow rifts versus wide rifts: Inferences for the mechanics of rifting from
922 laboratory experiments, *Philos. Trans. R. Soc. London, Ser. A*, 357, 695–712.
- 923
- 924 Brun, J. P., Beslier M.O., 1996. Mantle exhumation at passive margin, *Earth Planet. Sci. Lett.*,
925 142, 161– 173.
- 926
- 927 Brun, J.-P., and van den Driessche, J., 1994. Extensional gneiss domes and detachment fault
928 systems; structure and kinematics. *Bull. Société Géologique Fr.* 165, 519–530.
- 929
- 930 Brun, J.P., Wenzel, F. and ECORS-DEKORP team, 1991. Crustal structure of the southern
931 Rhine Graben from ECORS-DEKORP seismic reflection data, *Geology*, 19, 758–762. DOI:
932 10.1130/0091-7613(1991)019<0758:CSSOTS>2.3.CO
- 933
- 934 Brun, J.-P., Fort, X., 2011. Salt tectonics at passive margins: Geology versus models. *Mar. Pet.*
935 *Geol.* 28, 1123–1145. <https://doi.org/10.1016/j.marpetgeo.2011.03.004>

936

937 Brune, S., Heine, C., Pérez-Gussinyé, M., Sobolev, S.V., 2014. Rift migration explains
 938 continental margin asymmetry and crustal hyper-extension. *Nat. Commun.* 5.
 939 <https://doi.org/10.1038/ncomms5014>

940

941 Buck, W. R., 1991. Modes of continental lithospheric extension, *J. Geophys. Res.*, 96, 20,161–
 942 20,178.

943

944 Buck, W. R., F. Martinez, M. S. Steckler, and J. R. Cochran, 1988. Thermal consequences of
 945 lithospheric extension: Pure and simple, *Tectonics*, 7, 213 – 234.

946

947 Cadenas, P., Fernández-Viejo, G., 2017. The Asturian Basin within the North Iberian margin
 948 (Bay of Biscay): seismic characterisation of its geometry and its Mesozoic and Cenozoic
 949 cover. *Basin Res.* 29, 521–541. <https://doi.org/10.1111/bre.12187>

950

951 Canérot, J., 1988. Manifestations de l'halocinèse dans les Chaînons Béarnais (Zone Nord-
 952 Pyrénéenne) au Crétacé inférieur. *Comptes Rendus de l'Académie des Sciences de Paris* 306,
 953 1099-1102.

954

955 Canérot, J., 1989. Rifting éocétacé et halocinèse sur la marge ibérique des Pyrénées
 956 Occidentales (France). Conséquences structurales. *Bull. Cent. Rech. Explor.-Prod. Elf-*
 957 *Aquitaine* 13, 87–99.

958

959 Canérot, J., 2017. The pull apart-type Tardets-Mauléon Basin, a key to understand the
 960 formation of the Pyrenees. *Bull. Société Géologique Fr.* 188, 35.
 961 <https://doi.org/10.1051/bsgf/2017198>

962

963 Canérot, J., Hudec, M.R., Rockenbach, K., 2005. Mesozoic diapirism in the Pyrenean orogen:
 964 Salt tectonics on a transform plate boundary. *AAPG Bull.* 89, 211–229.
 965 <https://doi.org/10.1306/09170404007>

966

967 Canérot, J., Lenoble, J.-L., 1989. Le diapir du Lichançumendy (Pyrénées-Atlantiques), nouvel
 968 élément de la marge ibérique des Pyrénées occidentales. *Comptes Rendus Académie Sci.*
 969 *Sér. 2 Mécanique Phys. Chim. Sci. Univers Sci. Terre* 308, 1467–1472.

970

971 Canérot, J., Lenoble, J.-L., 1993. Diapirisme crétacé sur la marge ibérique des Pyrénées
 972 occidentales; exemple du pic de Lauriolle; comparaisons avec l'Aquitaine, les Pyrénées
 973 centrales et orientales. *Bull. Société Géologique Fr.* 164, 719–726.

974

975 Capdevila, R., Boillot, G., Lepvrier, C., Malod, J.-A., Mascle, G., 1980. Les formations
 976 cristallines du Banc Le Danois (marge nord ibérique). *Comptes Rendus Académie des*
 977 *Sciences de Paris* 291, 317–320.

978

979 Casas-Sainz, A.M., Gil-Imaz, A., 1998. Extensional subsidence, contractional folding and
 980 thrust inversion of the eastern Cameros basin, northern Spain. *Geol Rundsch* 86(4):802–818

981

982 Castanares, L.M., Robles, S., Gimeno, D. and Vicente Bravo, J.C., 2001. The Submarine

983 Volcanic System of the Errigoiti Formation (Albian-Santonian of the Basque-Cantabrian
 984 Basin, Northern Spain): Stratigraphic Framework, Facies, and Sequences. *Journ. Sedim.*
 985 *Research.* 71, 2, 318-333.

986

987 Chevrot, S., Sylvander, M., Díaz, J., Ruiz, M., Paul, A., PYROPE Working Group, 2015. The
 988 Pyrenean architecture as revealed by teleseismic P-to-S converted waves recorded along
 989 two dense transects. *Geophysical Journal International* 200, 1094-1105.

990

991 Chevrot, S., Sylvander, M., Diaz, J., Martin, R., Mouthereau, F., Manatschal, G., Masini, E.,
 992 Calassou, S., Grimaud, F., Pauchet, H., Ruiz, M., 2018. The non-cylindrical crustal architecture
 993 of the Pyrenees. *Sci. Rep.* 8. <https://doi.org/10.1038/s41598-018-27889-x>

994

995 Choukroune, P., 1976a. Strain patterns in the Pyrenean chain: *Philosophical Transactions of*
 996 *the Royal Society of London A: Mathematical, Physical and Engineering Sciences*, v. 283, no.
 997 1312, p. 271-280.

998

999 Choukroune, P., 1976b. Structure et évolution tectonique de la zone nord pyrénéenne,
 1000 *Mem. Soc. Geol. Fr.*, 127, 1-116.

1001

1002 Choukroune, P., ECORS Team, 1989. The ECORS Pyrenean deep seismic profile reflection
 1003 data and the overall structure of an orogenic belt. *Tectonics* 8, 23-39.

1004

1005 Choukroune, P., Mattauer, M., 1978. Tectonique des plaques et Pyrenees; sur le
 1006 fonctionnement de la faille transformante nord-pyreneenne; comparaisons avec des
 1007 modeles actuels. *Bull. Société Géologique Fr.* 7, 689-700.

1008

1009 Clerc, C., Lagabriele, Y., 2014. Thermal control on the modes of crustal thinning leading to
 1010 mantle exhumation: Insights from the Cretaceous Pyrenean hot paleomargins. *Tectonics* 33,
 1011 1340-1359. <https://doi.org/10.1002/2013TC003471>

1012

1013 Clerc, C., Jolivet, L., Ringenbach, J.-C., 2015a. Ductile extensional shear zones in the lower
 1014 crust of a passive margin. *Earth Planet. Sci. Lett.* 431, 1-7.
 1015 <https://doi.org/10.1016/j.epsl.2015.08.038>

1016

1017 Clerc, C., Lahfid, A., Monié, P., Lagabriele, Y., Chopin, C., Poujol, M., Boulvais, P.,
 1018 Ringenbach, J.C., Masini, E., de St Blanquat, M., 2015b. High-temperature metamorphism
 1019 during extreme thinning of the continental crust: a reappraisal of the North Pyrenean
 1020 passive paleomargin. *Solid Earth* 6, 643-668.

1021

1022 Clerc, C., Lagabriele, Y., Labaume, P., Ringenbach, J.-C., Vauchez, A., Nalpas, T., Bousquet, R.,
 1023 Ballard, J.-F., Lahfid, A., Fourcade, S., 2016. Basement – Cover decoupling and progressive
 1024 exhumation of metamorphic sediments at hot rifted margin. Insights from the Northeastern
 1025 Pyrenean analog. *Tectonophysics* 686, 82-97. <https://doi.org/10.1016/j.tecto.2016.07.022>

1026

1027 Clerc, C., Ringenbach, J.-C., Jolivet, L., Ballard, J.-F., 2018. Rifted margins: Ductile
 1028 deformation, boudinage, continentward-dipping normal faults and the role of the weak
 1029 lower crust. *Gondwana Res.* 53, 20-40. <https://doi.org/10.1016/j.gr.2017.04.030>

1921
1922
1923 1030
1924 1031 Corre, B., Lagabrielle, Y., Labaume, P., Fourcade, S., Clerc, C., Ballèvre, M., 2016.
1925 1032 Deformation associated with mantle exhumation in a distal, hot passive margin
1926 1033 environment: New constraints from the Sarailé Massif (Chaînons Béarnais, North-Pyrenean
1927 1034 Zone). *Comptes Rendus Geosci.* 348, 279–289. <https://doi.org/10.1016/j.crte.2015.11.007>
1928 1035
1929 1036 Cuevas, J., Tubia, J.M., 1999. The discovery of scapolite marbles in the Biscay Synclinorium
1930 1037 (Basque-Cantabrian basin, Western Pyrenees): geodynamic implications. *Terra Nova* 11,
1931 1038 259–265. <https://doi.org/10.1046/j.1365-3121.1999.00255.x>
1932 1039
1933 1040 Damotte, B., 1998. The ECORS Pyrenean Deep Seismic Surveys, 1985–1994, *Mémoires de la*
1934 1041 *Société géologique de France*, 173, 104 p., 8 pl.
1935 1042
1936 1043 Dañobeitia, J.J., Arguedas, M., Gallart, J., Banda, E., Makris, J., 1992. Deep crustal
1937 1044 configuration of the Valencia trough and its Iberian and Balearic borders from extensive
1938 1045 refraction and wide-angle reflection seismic profiling. *Tectonophysics* 203, 37–55.
1939 1046
1940 1047 Dauteuil, O., and Ricou, L.-E., 1989. Une circulation de fluides de haute-température à
1941 1048 l'origine du métamorphisme crétacé nord-pyrénéen. *Geodin. Acta* 3, 237–249.
1942 1049 <https://doi.org/10.1080/09853111.1989.11105190>
1943 1050
1944 1051 de Saint Blanquat, M., Bajolet, F., Grand'Homme, A., Proietti, A., Zanti, M., Boutin, A., Clerc,
1945 1052 C., Lagabrielle, Y., Labaume, P., 2016. Cretaceous mantle exhumation in the central
1946 1053 Pyrenees: New constraints from the peridotites in eastern Ariège (North Pyrenean zone,
1947 1054 France). *Comptes Rendus Geosci.* 348, 268–278. <https://doi.org/10.1016/j.crte.2015.12.003>
1948 1055
1949 1056 Debroas E.-J., 1978. Evolution de la fosse du flysch ardoisier de l'Albien supérieur au
1950 1057 Sénonien inférieur (zone interne métamorphique des Pyrénées navarro-languedociennes),
1951 1058 *Bull. Soc. Géol. Fr.* (7), XX, p. 639-648.
1952 1059
1953 1060 Debroas, E.J., 1990. Le flysch noir albo-cénomanién témoin de la structuration albienne à
1954 1061 sénonienne de la Zone nord-pyrénéenne en Bigorre (Hautes-Pyrénées, France). *Bull. Soc.*
1955 1062 *Geol. Fr.* VI, 273–285. <https://doi.org/10.2113/gssgfbull.VI.2.273>
1956 1063
1957 1064 DeFelipe, I., Pedreira, D., Pulgar, J.A., Iriarte, E., Mendia, M., 2017. Mantle exhumation and
1958 1065 metamorphism in the Basque-Cantabrian Basin (N Spain): Stable and clumped isotope
1959 1066 analysis in carbonates and comparison with ophicalcites in the North-Pyrenean Zone
1960 1067 (Urdach and Lherz). *Geochem. Geophys. Geosystems* 18, 631–652.
1961 1068 <https://doi.org/10.1002/2016GC006690>
1962 1069
1963 1070 Deramond, J., Souquet, P., Fondecave-Wallez, M.-J., Specht, M., 1993. Relationships
1964 1071 between thrust tectonics and sequence stratigraphy surfaces in foredeeps: model and
1965 1072 examples from the Pyrenees (Cretaceous-Eocene, France, Spain). *Geol. Soc. Lond. Spec.*
1966 1073 *Publ.* 71, 193–219.
1967 1074
1968 1075 Dercourt, J., Ricou, L. E., Vrielynck, B., 1993. Atlas Tethys Palaeoenvironmental maps Atlas
1969 1076 and Explanatory Notes, Gauthier Villars Ed. diffusion CGMW Paris, 307 p., 14 maps
1970
1971
1972
1973
1974
1975
1976
1977
1978
1979
1980

1077

1078 Dercourt, J., Zonenshain, L.P., Ricou, L.E. et al., 1986. Geological evolution of the Tethys belt
1079 from the Atlantic to the Pamirs since the Lias. *Tectonophysics*, 123, 1, 241-315.

1080

1081 Ducoux, M., Jolivet, L., Cagnard, F., Gumiaux, C., Baudin, T., Masini, E., Callot, J.P., Aubourg,
1082 C., Lahfid, A., Homonnay, E., 2019. The Nappe des Marbres unit of the Basque-Cantabrian
1083 basin: the tectono-thermal evolution of a fossil hyperextended rift basin. *Tectonics*
1084 submitted.

1085

1086 Duretz, T., Schmalholz, S.M., 2015. From symmetric necking to localized asymmetric
1087 shearing: the role of mechanical layering. *Geology*, 43, 8, 711-714.

1088

1089 Duretz, T., Petri, B., Mohn, G., Schmalholz, S.M., Schenker, F.L., Müntener, O., 2016. The
1090 importance of structural softening for the evolution and architecture of passive margins. *Sci.*
1091 *Rep.* 6, 38704. <https://doi.org/10.1038/srep38704>

1092

1093 Duretz, T., Asti, R., Lagabriele, Y., Brun, J.P., Jourdon, A., Clerc, C., Corre, B., 2019. Numerical
1094 modelling of syn-rift salt tectonics during Cretaceous Pyrenean Rifting. *Basin Research*, in
1095 press.

1096

1097 Espurt, N., Angrand, P., Teixell, A., Labaume, P., Ford, M., de Saint Blanquat, M., and Chevrot,
1098 S., 2019. Crustal-scale balanced cross-section and restorations of the Central Pyrenean belt
1099 (Nest- Cinca transect): superimposed orogenesis and Pyrenean rift system evolution.
1100 *Tectonophysics*, (to be completed)

1101

1102 Ethève, N., Mohn, G., Frizon de Lamotte, D., Roca, E., Tugend, J., Gómez-Romeu, J., 2018.
1103 Extreme Mesozoic Crustal Thinning in the Eastern Iberia Margin: The Example of the
1104 Columbrets Basin (Valencia Trough). *Tectonics* 37, 636–662.

1105

1106 Fabriès, J., Lorand, J.-P., Bodinier, J.-L., Dupuy, C., 1991. Evolution of the Upper Mantle
1107 beneath the Pyrenees: Evidence from Orogenic Spinel Lherzolite Massifs. *J. Petrol.*
1108 *Special_Volume*, 55–76. https://doi.org/10.1093/petrology/Special_Volume.2.55

1109

1110 Fabriès, J., Lorand, J.-P., Bodinier, J.-L., 1998. Petrogenetic evolution of orogenic lherzolite
1111 massifs in the central and western Pyrenees. *Tectonophysics* 292, 145–167.

1112

1113 Floquet, M., 1992. Outcrop sequence stratigraphy in a ramp setting: the Late Cretaceous
1114 Early Palaeogene deposits of the Castilian Ramp (Spain), Field Trip Guide Book in conjunction
1115 with the international symposium Sequence Stratigraphy of Mesozoic- Cenozoic European
1116 Basins: CNRS, Institut Français du Pétrole, Dijon. 130 p.

1117

1118 Frasca, G., Gueydan, F., Brun, J.-P., Monié, P., 2016. Deformation mechanisms in a
1119 continental rift up to mantle exhumation. Field evidence from the western Betics, Spain.
1120 *Mar. Pet. Geol.* 76, 310–328. <https://doi.org/10.1016/j.marpetgeo.2016.04.020>

1121

1122 Fügenschuh, B., Froitzheim, N., Capdevila, R., & Boillot, G. (2003). Offshore granulites from
1123 the Bay of Biscay margins: Fission tracks constrain a Proterozoic to Tertiary thermal history.

- 1124 Terra Nova, 15, 337–342, doi:10.1046/j.1365-3121.2003.00502.x.
- 1125
- 1126 Gallart, J., Rojas, H., Diaz, J., Dañobeitia, J.J., 1990. Features of deep crustal structure and the
 1127 onshore-offshore transition at the Iberian flank of the Valencia Trough (Western
 1128 Mediterranean). *J. Geodyn.* 12, 233–252.
- 1129
- 1130 García-Mondéjar J, Agirrezabala LM, Aranburu A, Fernández-Mendiola PA, Gómez-Pérez I,
 1131 López-Horgue M, Rosales I., 1996. Aptian–Albian tectonic pattern of the Basque–Cantabrian
 1132 Basin (Northern Spain). *Geol J* 31(1):13–45
- 1133
- 1134 García-Mondéjar J, Fernández-Mendiola PA, Agirrezabala LM, Aranburu A, López-Horgue
 1135 MA, Iriarte E, Martínez de Rituerto S., 2004. Extensión del Aptiense-Albiense en la Cuenca
 1136 Vasco-Cantábrica. SGEIGME, Madrid. Geological Society, London, Special Publications, 282,
 1137 111–138, 1 January, <https://doi.org/10.1144/SP282.6>
- 1138
- 1139 Gartrell, A.P., 1997. Evolution of rift basins and low-angle detachments in multilayer analog
 1140 models. *Geology* 25, 615–618. doi:10.1130/0091-7613(1997)025<0615:EORBAL>2.3.CO;2
- 1141
- 1142 Gernigon, L., Brönnert, M., Roberts, D., Olesen, O., Nasuti, A., Yamasaki, T., 2014. Crustal and
 1143 basin evolution of the southwestern Barents Sea: From Caledonian orogeny to continental
 1144 breakup: Evolution of the Barents Sea. *Tectonics* 33, 347–373.
- 1145 <https://doi.org/10.1002/2013TC003439>
- 1146
- 1147 Golberg, J.-M., Guiraud, M., Maluski, H., Séguret, M., 1988. Caractères pétrologiques et âge
 1148 du métamorphisme en contexte distensif du bassin sur décrochement de Soria (Crétacé
 1149 inférieur, Nord Espagne). *Comptes Rendus de l'Académie des Sciences Paris, Série* 11,307,
 1150 521–527.
- 1151
- 1152 Golberg, J.M., Leyreloup, A.F., 1990. High temperature-low pressure Cretaceous
 1153 metamorphism related to crustal thinning (Eastern North Pyrenean Zone, France). *Contrib.*
 1154 *Mineral. Petrol.* 104, 194–207. <https://doi.org/10.1007/BF00306443>
- 1155
- 1156 Gong, Z., Langereis, C.G., Mullender, T.A.T., 2008. The rotation of Iberia during the Aptian
 1157 and the opening of the Bay of Biscay. *Earth Planet. Sci. Lett.* 273, 80–93.
- 1158 <https://doi.org/10.1016/j.epsl.2008.06.016>
- 1159
- 1160 Grool, A. R., Ford, M., Vergés, J., Huisman, R. S., Christophoul, F., & Dielforder, A. (2018).
 1161 Insights into the crustal-scale dynamics of a doubly vergent orogen from a quantitative
 1162 analysis of its forelands: A case study of the Eastern Pyrenees. *Tectonics*, 37.
- 1163 <https://doi.org/10.1002/2017TC004731>
- 1164
- 1165 Guimerà, J., Alonso, Á., Mas, J.R., 1995. Inversion of an extensional-ramp basin by a newly
 1166 formed thrust: the Cameros basin (N. Spain).). in: *Basin Inversion* (J.G. Buchanan, P.G.
 1167 Buchanan, Eds). Geological Society, Special Publication, 88, 433–453.
- 1168 <https://doi.org/10.1144/GSL.SP.1995.088.01.23>
- 1169
- 1170 Guiraud, M., Séguret, M., 1985. A releasing solitary overstep model for the late Jurassic–

1171 early Cretaceous (Wealdian) Soria strike-slip basin (Northern Spain). In: Biddle KT, Christie-
1172 Blick N (eds) Strike slip deformation, basin formation and sedimentation, vol 37., SEPM
1173 Special Publication Society of Economic Paleontologists and Mineralogists, Tulsa, pp 159–
1174 175.
1175
1176 Hamilton, W., 1987. Crustal extension in the Basin and Range Province, southwestern United
1177 States. Geol. Soc. Lond. Spec. Publ. 28, 155–176.
1178 <https://doi.org/10.1144/GSL.SP.1987.028.01.12>
1179
1180 Huismans, R. S., Beaumont, C., 2007. Roles of lithospheric strain softening and heterogeneity
1181 in determining the geometry of rifts and continental margins
1182
1183 Huismans, R.S., Beaumont, C., 2011. Depth-dependent extension, two-stage breakup and
1184 cratonic underplating at rifted margins. Nature 473, 74–78.
1185 <https://doi.org/10.1038/nature09988>
1186
1187 Huismans, R.S., Beaumont, C., 2014. Rifted continental margins: The case for depth-
1188 dependent extension. Earth Planet. Sci. Lett. 407, 148–162. doi:10.1016/j.epsl.2014.09.032
1189
1190 James, V., Canérot, J., 1988. Diapirisme et structuration post-triasique des Pyrénées
1191 occidentales et de l'Aquitaine méridionale (France). Eclogae Geol. Helveticae 92, 63–72.
1192
1193 Jammes, S., Lavier, L., Manatschal, G., 2010a. Extreme crustal thinning in the Bay of Biscay
1194 and the Western Pyrenees: From observations to modeling. Geochem. Geophys.
1195 Geosystems 11. <https://doi.org/10.1029/2010GC003218>
1196
1197 Jammes, S., Tiberi, C., Manatschal, G., 2010b. 3D architecture of a complex transcurrent rift
1198 system: The example of the Bay of Biscay–Western Pyrenees. Tectonophysics 489, 210–226.
1199 <https://doi.org/10.1016/j.tecto.2010.04.023>
1200
1201 Jammes, S., Manatschal, G., Lavier, L., 2010c. Interaction between prerift salt and
1202 detachment faulting in hyperextended rift systems: The example of the Parentis and
1203 Mauléon basins (Bay of Biscay and western Pyrenees). AAPG Bull. 94, 957–975.
1204 <https://doi.org/10.1306/12090909116>
1205
1206 Jammes, S., Lavier, L.L., Reber, J.E., 2015. Localization and delocalization of deformation in a
1207 biminerale material. J. Geophys. Res. Solid Earth 120, 3649–3663.
1208 <https://doi.org/10.1002/2015JB011890>
1209
1210 Jammes, S., Lavier, L.L., 2016. The effect of biminerale composition on extensional processes
1211 at lithospheric scale. Geochem. Geophys. Geosystems 17, 3375–3392.
1212 <https://doi.org/10.1002/2016GC006399>
1213
1214 Jammes, S., Manatschal, G., Lavier, L., Masini, E., 2009. Tectono-sedimentary evolution
1215 related to extreme crustal thinning ahead of a propagating ocean: Example of the western
1216 Pyrenees. Tectonics 28. <https://doi.org/10.1029/2008TC002406>
1217

- 1218 Jolivet, L., Gorini, C., Smit, J., Leroy, S., 2015. Continental breakup and the dynamics of rifting
1219 in back-arc basins: The Gulf of Lion margin: Backarc rift and lower crust extraction. *Tectonics*
1220 34, 662–679. <https://doi.org/10.1002/2014TC003570>
- 1222 Lagabriele, Y., Bodinier, J.-L., 2008. Submarine reworking of exhumed sub-continental
1223 mantle rocks: field evidence from the Lherz peridotites, French Pyrenees: Cretaceous
1224 exhumation of pyrenean mantle. *Terra Nova* 20, 11–21. <https://doi.org/10.1111/j.1365-3121.2007.00781.x>
- 1227 Lagabriele, Y., Labaume, P., de Saint Blanquat, M., 2010. Mantle exhumation, crustal
1228 denudation, and gravity tectonics during Cretaceous rifting in the Pyrenean realm (SW
1229 Europe): Insights from the geological setting of the Iherzolite bodies. *Tectonics* 29.
1230 <https://doi.org/10.1029/2009TC002588>
- 1232 Lagabriele, Y., Clerc, C., Vauchez, A., Lahfid, A., Labaume, P., Azambre, B., Fourcade, S.,
1233 Dautria, J.-M., 2016. Very high geothermal gradient during mantle exhumation recorded in
1234 mylonitic marbles and carbonate breccias from a Mesozoic Pyrenean palaeomargin (Lherz
1235 area, North Pyrenean Zone, France). *Comptes Rendus Geosci.* 348, 290–300.
1236 <https://doi.org/10.1016/j.crte.2015.11.004>
- 1238 Lagabriele Y, Asti R, Fourcade S, Corre B, Poujol M, Uzel J, Labaume P, Clerc C, Lafay R,
1239 Picazo S, Maury R. 2019. Mantle exhumation at magma-poor passive continental margins.
1240 Part I. 3D architecture and metasomatic evolution of a fossil exhumed mantle domain
1241 (Urdach Iherzolite, north-western Pyrenees, France), *BSGF - Earth Sciences Bulletin* 190: 8.
1242 <https://doi.org/10.1051/bsgf/2019007>
- 1245 Lagabriele, Y., Asti, R., Fourcade, S., Corre, B., Uzel, J., Labaume, P., Clerc, C., Lafay, R.,
1246 Picazo, S., 2019b. The mechanisms of mantle exhumation at magma-poor passive
1247 continental margins. Part II. Insights from high-displacement, low-angle faults preserved in a
1248 fossil distal margin domain (Saraillé Iherzolites, north-western Pyrenees, France). *BSGF Earth*
1249 *Science Bull.*, in press.
- 1251 Le Pichon, X., Bonnin, J., Francheteau, J., Sibuet, J.C., 1971. Une hypothèse d'évolution
1252 tectonique du Golfe de Gascogne. *Hist. Struct. Golfe Gasc.* 2, 11–44.
- 1254 Lenoble, J.-L., Canérot, J., 1992. La lame extrusive de Pont Suzon (Zone Nord-Pyrénéenne en
1255 Vallée d'Aspe): reprise pyrénéenne d'une ride diapirique transverse d'âge crétacé. *Comptes*
1256 *Rendus Académie Sci. Sér. 2 Mécanique Phys. Chim. Sci. Univers Sci. Terre* 314, 387–391.
- 1258 Lister, G.S. and Davis, G.A. 1989. The origin of metamorphic core complexes and detachment
1259 faults formed during Tertiary continental extension in the northern Colorado River region,
1260 U.S.A. *Journal of Structural Geology*, Vol. 11, No. 112, pp. 65 to 94,
- 1262 Lister, G.S., Etheridge, M.A., Symonds, P.A., 1991. Detachment models for the formation of
1263 passive continental margins. *Tectonics* 10, 1038–1064.

1265 Lopez-Mir, B., Muñoz, J.A., García Senz, J., 2014. Restoration of basins driven by extension
1266 and salt tectonics: Example from the Cotiella Basin in the central Pyrenees. *J. Struct. Geol.*
1267 69, Part A, 147–162. <https://doi.org/10.1016/j.jsg.2014.09.022>
1268
1269 Manatschal, G., 2004. New models for evolution of magma-poor rifted margins based on a
1270 review of data and concepts from West Iberia and the Alps. *Int. J. Earth Sci.* 93.
1271 <https://doi.org/10.1007/s00531-004-0394-7>
1272
1273 Manatschal, G., Froitzheim, N., Rubenach, M., Turrin, B.D., 2001. The role of detachment
1274 faulting in the formation of an ocean-continent transition: insights from the Iberia Abyssal
1275 Plain. *Geol. Soc. Lond. Spec. Publ.* 187, 405–428.
1276 <https://doi.org/10.1144/GSL.SP.2001.187.01.20>
1277
1278 Manatschal, G., Engström, A., Desmurs, L., Schaltegger, U., Cosca, M., Müntener, O.,
1279 Bernoulli, D., 2006. What is the tectono-metamorphic evolution of continental break-up: The
1280 example of the Tasna Ocean–Continent Transition. *J. Struct. Geol.* 28, 1849–1869.
1281 <https://doi.org/10.1016/j.jsg.2006.07.014>
1282
1283 Mas, R., Benito MI, Arribas J, Alonso A, Arribas ME, González-Acebrón L, Hernán J, Quijada E,
1284 Suárez-González P, Omodeo Salè S (2011) Evolution of an intra-plate rift basin: the Latest
1285 Jurassic-Early Cretaceous Cameros Basin (Northwest Iberian Ranges, North Spain). In: Post-
1286 Meeting field trips 28th IAS Meeting, vol Geogúas 8. Zaragoza (Spain)
1287
1288 Masini, E., Manatschal, G., Tugend, J., Mohn, G., Flament, J.-M., 2014. The tectono-
1289 sedimentary evolution of a hyper-extended rift basin: the example of the Arzacq–Mauléon
1290 rift system (Western Pyrenees, SW France). *Int. J. Earth Sci.* 103, 1569–1596.
1291 <https://doi.org/10.1007/s00531-014-1023-8>
1292
1293 McClay, K., Muñoz, J.-A., García-Senz, J., 2004. Extensional salt tectonics in a contractional
1294 orogen: A newly identified tectonic event in the Spanish Pyrenees. *Geology* 32, 737–740.
1295 <https://doi.org/10.1130/G20565.1>
1296
1297 McKenzie, D., 1978. Some remarks on the development of sedimentary basins. *Earth Planet.*
1298 *Sci. Lett.* 40, 25–32. [https://doi.org/10.1016/0012-821X\(78\)90071-7](https://doi.org/10.1016/0012-821X(78)90071-7)
1299
1300 Mendia, M., and Gil Ibarguchi, J. I. 1991. High-grade metamorphic rocks and peridotites
1301 along the Leiza Fault (Western Pyrenees, Spain), *Geologische Rundschau* 80/1.
1302
1303 Michon, L. and Merle, O. 2003. Mode of lithospheric extension: Conceptual models from
1304 analogue modeling. *Tectonics*, 22 (4), pp.1028. <https://doi.org/10.1029/2002TC001435>
1305
1306 Mohn, G., Karner, G.D., Manatschal, G., Johnson, C.A., 2015. Structural and stratigraphic
1307 evolution of the Iberia–Newfoundland hyper-extended rifted margin: a quantitative
1308 modelling approach. *Geol. Soc. Lond. Spec. Publ.* 413, 53–89.
1309 <https://doi.org/10.1144/SP413.9>
1310

- 1311 Mohn, G., Manatschal, G., Beltrando, M., Masini, E., Kuszniir, N., 2012. Necking of continental
1312 crust in magma-poor rifted margins: Evidence from the fossil Alpine Tethys margins: Necking
1313 of continental crust. *Tectonics* 31, n/a-n/a. <https://doi.org/10.1029/2011TC002961>
1314
- 1315 Mohn, G., Manatschal, G., Müntener, O., Beltrando, M., Masini, E., 2010. Unravelling the
1316 interaction between tectonic and sedimentary processes during lithospheric thinning in the
1317 Alpine Tethys margins. *Int. J. Earth Sci.* 99, 75–101. [https://doi.org/10.1007/s00531-010-](https://doi.org/10.1007/s00531-010-0566-6)
1318 0566-6
1319
- 1320 Monchoux, P., 1970. Les lherzolites pyrénéennes: contribution à l'étude de leur minéralogie,
1321 de leur genèse et de leurs transformations. Université Paul Sabatier de Toulouse (Sciences).
1322
- 1323 Muñoz, J.A., 1992. Evolution of a continental collision belt: ECORS-Pyrenees crustal balanced
1324 cross-section, in: *Thrust Tectonics*. Springer, pp. 235–246.
1325
- 1326 Nagel, T. J. and Buck, W. R., 2004. Symmetric alternative to asymmetric rifting models.
1327 *Geology*, 32, 11. pp 937-940 Doi 10.1130/G20785.1
1328
- 1329 Olivet, J.L., 1996. La cinématique de la plaque ibérique. *Bull Cent Rech Explor Prod Elf*
1330 *Aquitaine* 20, 131–195.
1331
- 1332 Omodeo Salè, S., Guimerà, J., Mas, R., & Arribas, J. (2014). Tectono-stratigraphic evolution of
1333 an inverted extensional basin: The Cameros Basin (north of Spain). *International Journal of*
1334 *Earth Sciences*, 103(6), 1597–1620. <https://doi.org/10.1007/s00531-014-1026-5>
1335
- 1336 Ortí, F., Pérez-López, A., Salvany, J.M., 2017. Triassic evaporites of Iberia: Sedimentological
1337 and palaeogeographical implications for the western Neotethys evolution during the Middle
1338 Triassic–Earliest Jurassic. *Palaeogeogr. Palaeoclimatol. Palaeoecol.* 471, 157–180.
1339 <https://doi.org/10.1016/j.palaeo.2017.01.025>
1340
- 1341 Osmundsen, P.T., Ebbing, J., 2008. Styles of extension offshore mid-Norway and implications
1342 for mechanisms of crustal thinning at passive margins: STYLES OF EXTENSION OFFSHORE
1343 NORWAY. *Tectonics* 27, n/a-n/a. <https://doi.org/10.1029/2007TC002242>
1344
- 1345 Osmundsen, P.T., Péron-Pinvidic, G., 2018. Crustal-Scale Fault Interaction at Rifted Margins
1346 and the Formation of Domain-Bounding Breakaway Complexes: Insights From Offshore
1347 Norway. *Tectonics* 37, 935–964. <https://doi.org/10.1002/2017TC004792>
1348
- 1349 Pedrera, A., García-Senz, J., Ayala, C., Ruiz-Constán, A., Rodríguez-Fernández, L. R., Robador,
1350 A., & GonzálezMenéndez, L. (2017). Reconstruction of the exhumed mantle across the North
1351 Iberian Margin by crustal-scale 3-D gravity inversion and geological cross section. *Tectonics*,
1352 36. <https://doi.org/10.1002/2017TC004716>
1353
- 1354 Péron-Pinvidic, G., Manatschal, G., Minshull, T.A., Sawyer, D.S., 2007. Tectonosedimentary
1355 evolution of the deep Iberia-Newfoundland margins: Evidence for a complex breakup
1356 history. *Tectonics* 26, 1–19. <https://doi.org/10.1029/2006TC001970>
1357

1358 Péron-Pinvidic, G., Manatschal, G., 2009. The final rifting evolution at deep magma-poor
1359 passive margins from Iberia-Newfoundland: a new point of view. *Int. J. Earth Sci.* 98, 1581–
1360 1597. <https://doi.org/10.1007/s00531-008-0337-9>
1361
1362 Pinet, B., Montadert, L., ECORS Scientific Party, 1987. Deep seismic reflection and refraction
1363 profiling along the Aquitaine shelf (Bay of Biscay). *Geophys. J. Int.* 89, 305–312.
1364 <https://doi.org/10.1111/j.1365-246X.1987.tb04423.x>
1365
1366 Puigdefàbregas, C., Souquet, P., 1986. Tecto-sedimentary cycles and depositional sequences
1367 of the Mesozoic and Tertiary from the Pyrenees. *Tectonophysics* 129, 173–203.
1368
1369 Rat, P., 1988. The Basque–Cantabrian basin between the Iberian and European plates: some
1370 facts but still many problems. *Rev Soc Geol Esp* 1(3–4):327–348
1371
1372 Rat, P., Amiot, M., Feuillée, P., Floquet, M., Mathey, B., Pascal, A., Salomon, J., García
1373 Mondéjar, J., Pujalte, J., Lamolda, M., et al., 1983. Vue sur le Cretacé basco-cantabrique et
1374 nord-ibérique. Une marge, son arrière-pays, ses environ. sédimentaires. *Mémoires Géol.*
1375 *Univ. Dijon* 9, 191.
1376
1377 Rat, J., Mouthereau, F., Brichau, S., Crémades, A., Bernet, M., Balvay, M., Ganne, J., Lahfid,
1378 A., Gautheron, C., 2019. Tectonothermal Evolution of the Cameros Basin: Implications for
1379 Tectonics of North Iberia. *Tectonics* 38, 440–469. <https://doi.org/10.1029/2018TC005294>
1380
1381 Ravier, J., 1959. Le métamorphisme des terrains secondaires des Pyrénées. *Mémoires de la*
1382 *Société Géologique de France*, N° 86, 250 p., 19 flg., 9 pl. phot.
1383
1384 Reston, T., McDermott, K., 2014. An assessment of the cause of the ‘extension discrepancy’
1385 with reference to the west Galicia margin. *Basin Res.* 26, 135–153.
1386 <https://doi.org/10.1111/bre.12042>
1387
1388 Reston, T.J., 1988. Evidence for shear zones in the lower crust offshore Britain. *Tectonics* 7,
1389 929–945. <https://doi.org/10.1029/TC007i005p00929>
1390
1391 Reston, T.J., Krawczyk, C.M., Hoffmann, H.-J., 1995. Detachment tectonics during Atlantic
1392 rifting: analysis and interpretation of the S reflection, the west Galicia margin. *Geol. Soc.*
1393 *Lond. Spec. Publ.* 90, 93–109. <https://doi.org/10.1144/GSL.SP.1995.090.01.05>
1394
1395 Reston, T.J., Pérez-Gussinyé, M., 2007. Lithospheric extension from rifting to continental
1396 breakup at magma-poor margins: rheology, serpentinisation and symmetry. *Int. J. Earth Sci.*
1397 96, 1033–1046. <https://doi.org/10.1007/s00531-006-0161-z>
1398
1399 Roca, E., Muñoz, J.A., Ferrer, O., Ellouz, N., 2011. The role of the Bay of Biscay Mesozoic
1400 extensional structure in the configuration of the Pyrenean orogen: Constraints from the
1401 MARCONI deep seismic reflection survey. *Tectonics* 30.
1402 <https://doi.org/10.1029/2010TC002735>
1403

- 1404 Roma, M., Ferrer, O., Roca, E., Pla, O., Escosa, F., Butillé, M., 2018. Formation and inversion
1405 of salt-detached ramp-syncline basins. Results from analog modeling and application to the
1406 Columbrets Basin (Western Mediterranean), *Tectonophysics* 10.1016/j.tecto.2018.08.012
- 1408 Roure, F., Choukroune, P., 1998. Contribution of the ECORS seismic data to the Pyrenean
1409 geology: Crustal architecture and geodynamic evolution of the Pyrenees. *Mém. Société*
1410 *Géologique Fr.* 173, 37–52.
- 1412 Rowan, M.G., 2014. Passive-margin salt basins: hyperextension, evaporite deposition, and
1413 salt tectonics. *Basin Res.* 26, 154–182. <https://doi.org/10.1111/bre.12043>
- 1415 Ruiz, M., 2007. Caracterització estructural i sismotectònica de la litosfera en el Domini
1416 Pirenaico-Cantàbric a partir de mètodes de sísmica activa i passiva, Ph.D. thesis, Univ. of
1417 Barcelona, Barcelona, Spain.
- 1419 Salas, R., Casas, A., 1993. Mesozoic extensional tectonics, stratigraphy and crustal evolution
1420 during the Alpine cycle of the eastern Iberian basin. *Tectonophysics* 228, 33–55.
1421 [https://doi.org/10.1016/0040-1951\(93\)90213-4](https://doi.org/10.1016/0040-1951(93)90213-4)
- 1423 Salas, R., Guimerà, J., Mas, R., Martín-Closas, C., Meléndez, A., Alonso, Á., 2001. Evolution of
1424 the Mesozoic Central Iberian Rift System and its Cainozoic inversion (Iberian chain). In:
1425 Ziegler PA, Cavazza W, Robertson AHF, Crasquin-Soleau S (eds), *Peri-Tethys Memoir 6: Peri-*
1426 *Tethyan Rift/Wrench Basins and Passive Margins*, vol 186. *Mémoires du Museum National*
1427 *d'Histoire Naturelle*, Paris, pp 145–186
- 1429 Saspiturry, N., Razin, P., Baudin, T., Serrano, O., Issautier, B., Lasseur, E., Allanic, C., Thion, I.,
1430 Leleu, S., 2019. Symmetry vs. asymmetry of a hyper-thinned rift: Example of the Mauléon
1431 Basin (Western Pyrenees, France). *Mar. Pet. Geol.* 104, 86–105.
1432 <https://doi.org/10.1016/j.marpetgeo.2019.03.031>
- 1434 Saura, E., Ardèvol i Oró, L., Teixell, A., Vergés, J., 2016. Rising and falling diapirs, shifting
1435 depocenters, and flap overturning in the Cretaceous Sopeira and Sant Gervàs subbasins
1436 (Ribagorça Basin, southern Pyrenees): Southern Pyrenees Cretaceous Diapirism. *Tectonics*
1437 35, 638–662. <https://doi.org/10.1002/2015TC004001>
- 1439 Scotese, C.R. and Schettino, A., 2017. Late Permian-Early Jurassic paleogeography of
1440 Western Tethys and the world. In Soto et al., eds, *Permo-Triassic salt provinces of Europe,*
1441 *North Africa and the Atlantic margins. Tectonics and Hydrocarbon potential.* Elsevier, pp. 57-
1442 91.
- 1444 Sibuet, J.-C., Srivastava, S.P., Spakman, W., 2004. Pyrenean orogeny and plate kinematics. *J.*
1445 *Geophys. Res. Solid Earth* 109, B08104. <https://doi.org/10.1029/2003JB002514>
- 1447 Soto, J.I., Flinch, J.F. and Tari, G., 2017. Permo-Triassic salt provinces of Europe, North Africa
1448 and the Atlantic margins: A synthesis. In Soto et al., eds, *Permo-Triassic salt provinces of*
1449 *Europe, North Africa and the Atlantic margins. Tectonics and Hydrocarbon potential.*
1450 Elsevier, pp. 3-41.

1451

1452 Sutra, E., Manatschal, G., Mohn, G., Unternehr, P., 2013. Quantification and restoration of
1453 extensional deformation along the Western Iberia and Newfoundland rifted margins. *Geoch.*
1454 *Geoph. Geosys.* 14 (8), 2575e2597.

1455

1456 Teixell, A., 1998. Crustal structure and orogenic material budget in the west central
1457 Pyrenees. *Tectonics* 17, 395–406. <https://doi.org/10.1029/98TC00561>

1458

1459 Teixell, A., Labaume, P., Lagabrielle, Y., 2016. The crustal evolution of the west-central
1460 Pyrenees revisited: Inferences from a new kinematic scenario. *Comptes Rendus Geosci.* 348,
1461 257–267. <https://doi.org/10.1016/j.crte.2015.10.010>

1462

1463 Teixell, A., Labaume, P., Ayarza, P., Espurt, N., de Saint Blanquat, M., Lagabrielle, Y., 2018.
1464 Crustal structure and evolution of the Pyrenean-Cantabrian belt: A review and new
1465 interpretations from recent concepts and data. *Tectonophysics* 724, 146–170.
1466 <https://doi.org/10.1016/j.tecto.2018.01.009>

1467

1468 Thiébaud J., Durand-Wackenheim C., Debeaux M. and Souquet P., 1992. Métamorphisme
1469 des évaporites triasiques du versant nord des Pyrénées centrales et occidentales. *Bull. Soc.*
1470 *Hist. Nat. Toulouse.* 128, 77-84.

1471

1472 Thinon, I., Matias, L., Réhault, J.P., Hirn, A., Fidalgo-González, L., Avedik, F., 2003. Deep
1473 structure of the Armorican Basin (Bay of Biscay): a review of Norgasis seismic reflection and
1474 refraction data. *J. Geol. Soc.* 160, 99–116. <https://doi.org/10.1144/0016-764901-103>

1475

1476 Tirel, C., Brun, J.-P. and Burov, E., 2008. Dynamics and structural development of
1477 metamorphic core complexes. *Journal of Geophysical Research*, 113(B4): B04403.

1478

1479 Tomassimo, A., Marillier, F., 1997. Processing and interpretation in the tau-p domain of the
1480 ECORS Bay of Biscay expanding spread profiles. *Mém. Société Géologique Fr.* 171, 31–43.

1481

1482 Tugend, J., Manatschal, G. and Kusznir, N.J., 2015. Spatial and temporal evolution of
1483 hyperextended rift systems: Implication for the nature, kinematics, and timing of the
1484 Iberian-European plate boundary, *Geology*, 43(1), 15–18, doi:10.1130/G36072.1.

1485

1486 Tugend, J., Manatschal, G., Kusznir, N.J., Masini, E., Mohn, G., Thinon, I., 2014. Formation
1487 and deformation of hyperextended rift systems: Insights from rift domain mapping in the
1488 Bay of Biscay-Pyrenees. *Tectonics* 33, 1239–1276. <https://doi.org/10.1002/2014TC003529>

1489

1490 Vergés, J., García-Senz, J., 2001. Mesozoic evolution and Cainozoic inversion of the Pyrenean
1491 rift. *Mém. Muséum Natl. Hist. Nat.* 186, 187–212.

1492

1493 Vielzeuf, D., Kornprobst, J., 1984. Crustal splitting and the emplacement of Pyrenean
1494 Iherzolites and granulites. *Earth Planet. Sci. Lett.* 67, 87–96. [https://doi.org/10.1016/0012-821X\(84\)90041-4](https://doi.org/10.1016/0012-821X(84)90041-4)

1496

1497 Vissers, R.L.M., Drury, M.R., Newman, J. and Fliervoet, T.F., 1997. Mylonitic deformation in

1498 upper mantle peridotites of the North Pyrenean Zone (France) : implications for strength
1499 and strain localization in the lithosphere. *Tectonophysics*, 279, 303-325.
1500
1501 Wang, Y., Chevrot, S., Monteiller, V., Komatitsch, D., Mouthereau, F., Manatschal, G.,
1502 Sylvander, M., Diaz, J., Ruiz, M., Grimaud, F., Benahmed, S., Pauchet, H., Martin, R., 2016.
1503 The deep roots of the western Pyrenees revealed by full waveform inversion of teleseismic P
1504 waves. *Geology* 44, 475–478. <https://doi.org/10.1130/G37812.1>
1505
1506 Wernicke, B., 1981. Low-angle normal faults in the Basin and Range Province: nappe
1507 tectonics in an extending orogen. *Nature* 291, 645–648. <https://doi.org/10.1038/291645a0>
1508
1509 Wernicke, B., 1985. Uniform-sense normal simple shear of the continental lithosphere. *Can.*
1510 *J. Earth Sci.* 22, 108–125. <https://doi.org/10.1139/e85-009>
1511
1512 Ziegler, 1988. Evolution of Arctic-North Atlantic and western Tethys. Tulsa. AAPG Memoir,
1513 43, 198 pp.
1514
1515 Zamora, G., Fleming, M., Gallastegui, J., 2017. Salt Tectonics Within the Offshore Asturian
1516 Basin: North Iberian Margin, in Soto, J.I, Flinch, J.F. and Tari, G., 2017. Permo-Triassic salt
1517 provinces of Europe, North Africa and the Atlantic margins: A synthesis. In Soto et al., eds,
1518 Permo-Triassic salt provinces of Europe, North Africa and the Atlantic margins. *Tectonics and*
1519 *Hydrocarbon potential*. Elsevier, pp. 353-367.
1520
1521
1522

1523 **Figure captions**

1524

1525 **Figure 1. Location of the studied basins and their paleogeographic position during the**
1526 **Cretaceous at the onset of the Iberia drift.**

1527 (a) Simplified structural map of the Cantabrian-Pyrenean orogenic system and adjoining
1528 Iberia showing Eurasia deformed and undeformed domain (modified from Verges and Garcia-
1529 Senz, 2001 and Teixell et al., 2018). (b) Hypothetical reconstruction at the onset of the Iberia
1530 drift (modified after Tugend et al., 2014).

1531

1532 **Figure 2. A compilation of Cretaceous basins architecture from the Cantabrian-Pyrenean**
1533 **belt.**

1534 Reconstructions from field and geophysical data collected by various authors in the Basque-
1535 Cantabrian basin (a, b, c) and in the North Pyrenean Zone (NPZ): Mauléon basin (d),
1536 Chainons Béarnais (e, f), Baronnies basin (g) and Agly massif-Boucheville basin (h).

1537

1538 **Figure 3. Structure and evolution of Iberia-Newfoundland-type and Alpine-type passive**
1539 **margins** (modified from Péron-Pinvidic and Manatschal, 2009 and Mohn et al., 2012).

1540 (a): two sketches showing the main concepts linked to Iberia-Newfoundland-type margin
1541 evolution, namely: (i) strong final asymmetry with upper and lower plates separated by a
1542 single detachment fault (HHD, Hobby High detachment), (ii) emplacement of extensional
1543 allochthons as rigid crustal blocks over the exhumed mantle. (b): strain distribution and
1544 strain partitioning during lithospheric thinning at magma-poor rifted margin, with example
1545 from the fossil Alpine Tethys margin. In this model, the pre-rift cover remains welded on the
1546 tilted crustal blocks; the middle crust is thinned to zero and the upper crust and upper
1547 mantle are juxtaposed at the break up stage. The concepts shown in (a) and (b) contrast with
1548 the concepts attached to the smooth-slopes basins evolution developed in this paper.

1549

1550 **Figure 4. The geological record of the Cretaceous extension in the Paleozoic basement and**
1551 **exhumed mantle of the North Pyrenean Zone (NPZ).**

1552 The map shows the location of mantle bodies and crustal units illustrated in photographs a
1553 to k. (a): dated crustal mylonites associated with the Urdach Iherzolites; thin section

1554 microphotograph (natural light) of the leucocratic gneissic mylonite exposed at Col d'Urdach
 1555 and containing numerous micafishes (dating by the Ar/Ar method at 105 Ma; after Asti et al.,
 1556 2019). (b): thin section of typical ultramylonite from the lenses of Paleozoic material welded
 1557 on the exhumed mantle rocks of the Saraillé lherzolite (Asti et al., 2019). (c): phacoidal fabric
 1558 defined by anastomosing shear zones in the mantle body of Bestiac. This fabric is typical of
 1559 the lenticular layer as defined by Lagabriele et al. (2019a, 2019b). (d): phacoidal fabric in the
 1560 lenticular layer of the lherzolite body of Moncaup. (e): phacoidal fabric in the lenticular layer
 1561 of the lherzolite body of Saraillé (Lagabriele et al., 2019b). (f): curved shear zones and
 1562 elongated tectonic lenses in serpentinized lherzolites of the lenticular layer in the Moncaut
 1563 peridotite body. (g and h): phacoidal fabric in the lenticular layer of the lherzolite body of
 1564 Urdach: h shows pervasive carbonation (Lagabriele et al., 2019a). (i and j): thin section and
 1565 outcrop of anastomosing serpentinized shear bands in the lherzolites of Etang de Lers
 1566 (Lherz). (k): anastomosing serpentinized shear bands in the lherzolites of Avezac.

1567

1568 **Figure 5. The geological record of the Cretaceous extension in the pre-rift cover of the**
 1569 **metamorphic North Pyrenean Zone (NPZ). Some field view of outcrops showing the layer**
 1570 **perpendicular flattening and the S0/S1 syn-metamorphic foliation.**

1571 (a): layer-parallel boudinage in the Calce quarry (Jurassic dolostones of the Agly massif
 1572 cover, Eastern NPZ). (b): layer-parallel ductile stretching of the meta-laterite and carbonate
 1573 breccia in the Benou quarry near Turon de la Tecouère lherzolite body (Chainons Béarnais,
 1574 Western NPZ). (c): flattened fossils in the Jurassic meta-dolostones of the Saleix valley (Aulus
 1575 basin, Central NPZ). (d): extreme stretching of a rudist-rich Urgonian marbles at Sarrance
 1576 (Chainons Béarnais, Western NPZ) (see also fig. 6c). (e): tight normal faults affecting the
 1577 early S0/S1 syn-metamorphic foliation in the pre-rift cover marbles of the Agly massif. These
 1578 features characterize the ductile-brittle transition that occurred at the end of the rifting
 1579 history. (f): same features as (e) but in the marbles of the detached Lherz body cover
 1580 (southern side). (g): recumbent folds associated with the early ductile foliation in marbles
 1581 from the detached cover of the Pays de Sault Paleozoic basement (Eastern NPZ). (h): tectonic
 1582 brecciation with calcite veining marking the ductile-brittle transition in the marbles of the
 1583 Lherz body cover (western side).

1584

1585 **Figure 6 . A theoretical log of the lithological succession in the internal domain of the**

2701
2702
2703 **1586 Cretaceous NPZ rift basins.**
2704

2705 1587 The photographs illustrate the various rock-types forming the basin basement (crust and
2706 1588 mantle) and the pre-rift and syn-rift series. (a): Chaînons Béarnais (Saraillé massif, western
2707 1589 NPZ). (b): Boucheville basin (eastern NPZ). (c): Urgonian at Sarrance (western NPZ) (see also
2710 1590 fig. 5d). (d): Jurassic dolomites at Calce (eastern NPZ). (e): base of pre-rift series (Bestiac,
2711 1591 eastern NPZ). (f): base of pre-rift series (Moncaup, central NPZ). (g): crustal lenses of Saraillé
2713 1592 massif (western NPZ). (h): lenticular layer (Urdach mantle body, western NPZ).
2714

2715 1593

2716
2717 **1594 Figure 7. Interpreted and reconstructed profiles of peri-Pyrenean Cretaceous basins**
2718 **1595 architecture.**
2719

2720 1596 (a): Parentis basin. (b): Columbrets basin. (c and d): Cameros basin. See location of basins in
2721 1597 fig. 1.
2722

2723 1598

2724
2725 **1599 Figure 8. A compilation of model results and conceptual representations of extended to**
2726 **1600 hyper-extended continental crust.**
2727

2728 1601 This compilation aims enhancing the main mechanical concepts involved in the processes of
2729 1602 crustal extension and how they apply or not apply to the genesis and evolution of the
2730 1603 smooth-slopes basins defined in this article (see text for discussion).
2731
2732
2733

2734 1604

2735 **1605 Figure 9. A compilation of reconstructed architecture of Pyrenean Cretaceous basins and a**
2736 **1606 Basque-Parentis transect.**
2737

2738 1607 All represented sections are based on the activation of a restricted number of detachment
2739 1608 faults. As discussed in text, such representations do not match the newly defined smooth-
2740 1609 slopes architecture that characterize the Pyrenean and peri-Pyrenean Cretaceous basins.
2741
2742
2743

2744 1610

2745 **1611 Figure 10. Deformation regimes of the various units composing a typical smooth-slopes**
2746 **1612 basin.**
2747

2748 1613 (a): distribution of pure shear and simple shear regimes in a simplified smooth-slopes basin
2749 1614 system. (b): Detail of the very distal part of the hyper-extended crust (area shown in a). (b1):
2750 1615 simplified log showing the association of metric to hectometric crustal lenses separated
2751 1616 from the mantle rocks by the crust-mantle detachment and from the detached pre-rift cover
2752 1617 by the cover décollement (see definition in Lagabrielle et al., 2019a, 2019b). (b2): field view
2753
2754
2755
2756
2757
2758
2759
2760

1618 of crustal sheets from the base of the Saraillé massif (western NPZ). (b3): field view of
1619 anastomosing shear zones cutting through the serpentinitized peridotite of the Saraillé body
1620 and forming the lenticular layer of the crust-mantle detachment (see also fig. 4c to k).

1621

1622 **Figure 11. A compilation of schematic architecture of selected Atlantic and Mediterranean**
1623 **passive margins.**

1624 These margin profiles are selected because they offer architectures which do not fit with
1625 the Iberia-Newfoundland-type margin (see fig. 2). In particular, they show large scale crustal
1626 boudinage and lenticulation that are consistent with a ductile regime of extensional
1627 deformation. Sheets of hyper thinned crustal material is indicated by the orange arrow (see
1628 comments in text). Note that scale is similar in all profiles.

1629

1630 **Figure 12. Three numerical models of rift development compared to the Angola-Brazil and**
1631 **Iberia transects.**

1632 All models highlight a mode of deformation that leads to the development of very thin and
1633 long sheets of crustal material also observed in the Angola-Campos transect but not in the
1634 Iberia transect. Such deformation necessarily imply a ductile behaviour of the crust
1635 consistent with processes acting in the central part of the smooth-slopes basins studied in
1636 this paper (see text for further comments).

1637

1638 **Figure 13. Paleogeography of Triassic deposits and Cretaceous rifting around the Iberia**
1639 **plate.**

1640 (a): paleogeographic maps for the Triassic period (modified from Orti et al., 2017) and
1641 location of some further Cretaceous rifted regions. Note that by contrast to the area where
1642 Cretaceous smooth-slopes basins will open, the area corresponding to the future Iberia-
1643 Newfoundland conjugate margins are devoid of thick evaporitic series. (b): paleogeographic
1644 maps for the Ladinian and Carnian (Middle-early Late Triassic times, 242-227 Ma) modified
1645 after Scotese and Schettino (2017). (c): paleogeography of Upper Triassic deposits prepared
1646 after a compilation of unpublished data by D. Frizon de Lamotte (pers. com.) superimposed
1647 on a plate reconstruction by Olivet (1996).

1648

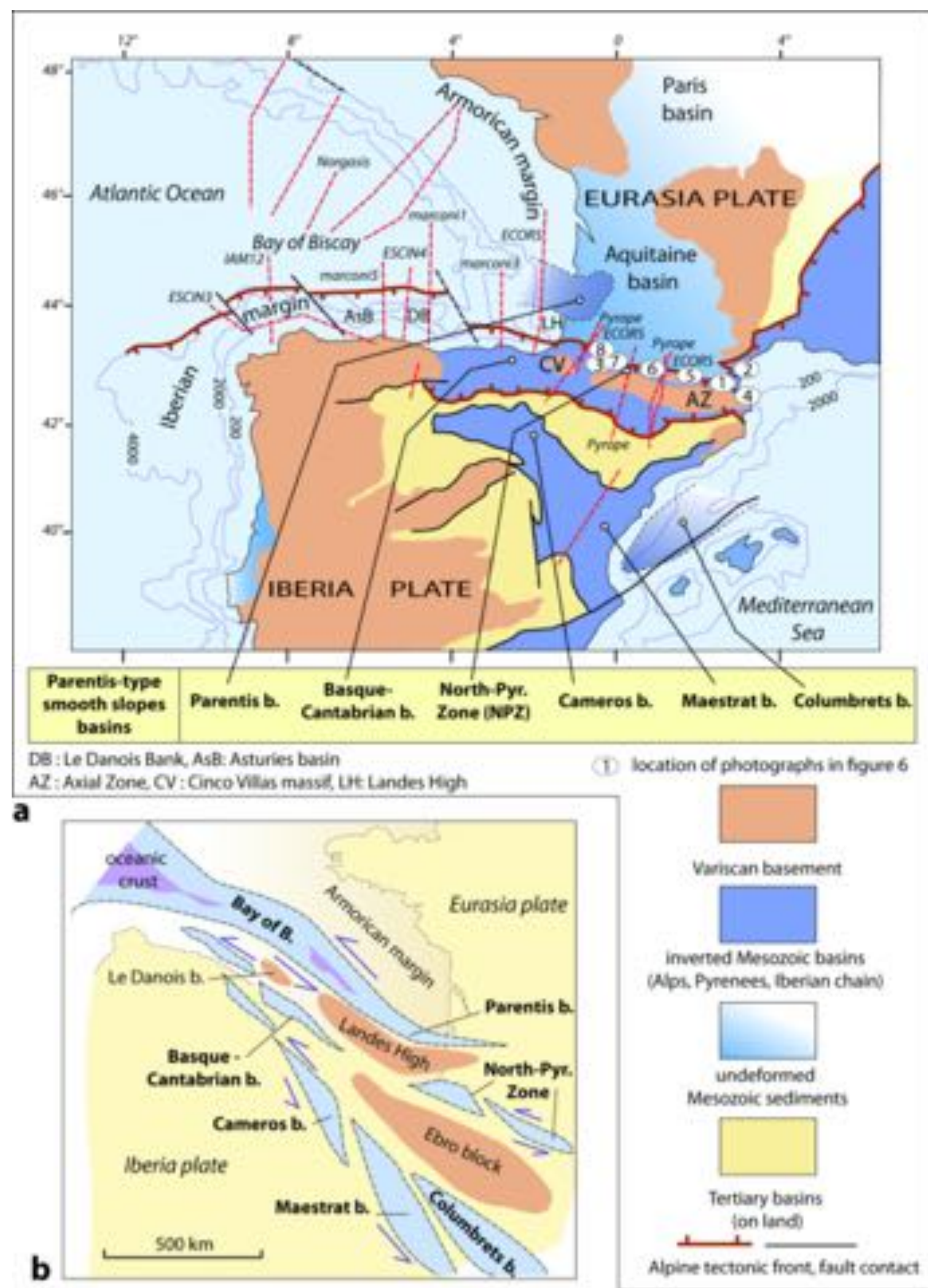
Figure 14. Correlation between the paleogeography of Triassic deposits and the mode of rifting around the Iberia plate.

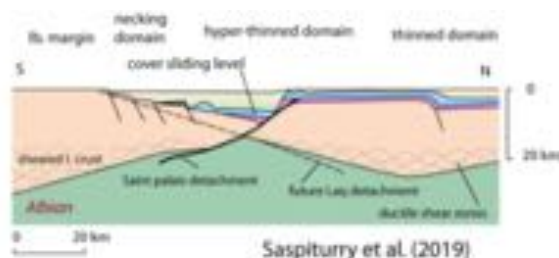
(a): cartoons (a1 and a2) illustrating the contrasted rifting modes between the Iberia-Newfoundland-type and the Parentis-type margins (modified from Clerc and Lagabriele, 2014). (b): paleogeography of Triassic (Late Norian) deposits according to Marcoux et al. in the Dercourt et al. (1993) map atlas. As paleogeographic maps in fig. 13, this reconstruction points to the lack of thick evaporites deposits in the future Iberia-Newfoundland rifting domain (see text for discussion).

Figure 15. Time-dependent rheological evolution of the Pyrenean rifting based on geological constraints from the North Pyrenean Zone and numerical results from a thermo-mechanical numerical modeling.

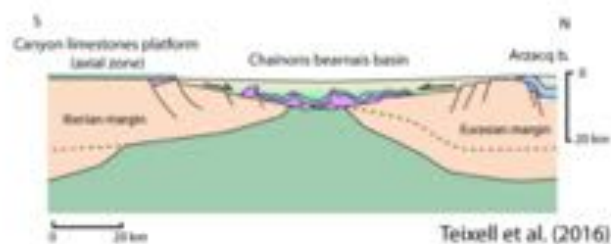
Sketches depicting the geological evolution are extracted from the Clerc et al. (2016) model. Rheological profiles derive from the Duretz et al., (2019) model. They are placed at critical locations (1, 2 and 3) of the rift in order to emphasize the drastic changes in the mechanical behaviour during its evolution from limited crustal extension to local mantle exhumation (see detailed description in text).

Figure 16. A theoretical structural model for the Cantabrian, Pyrenean and Iberian symmetrical smooth-slopes basins based on the features and concepts discussed in this article.





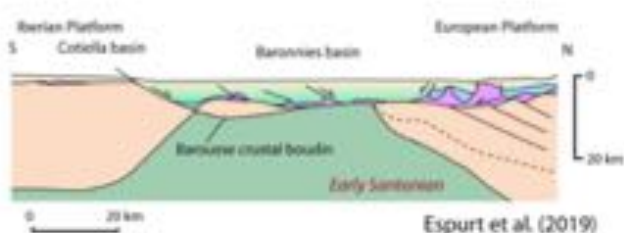
a. Western North Pyrenean Zone (1)



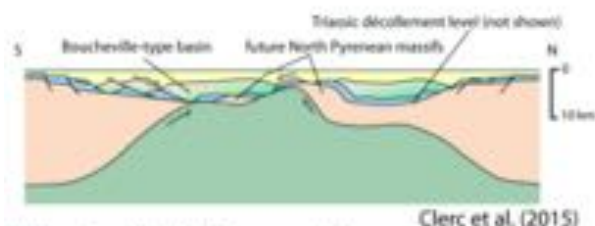
b. Western North Pyrenean Zone (2)



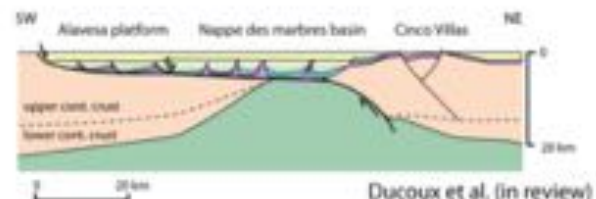
c. Western North Pyrenean Zone (3)



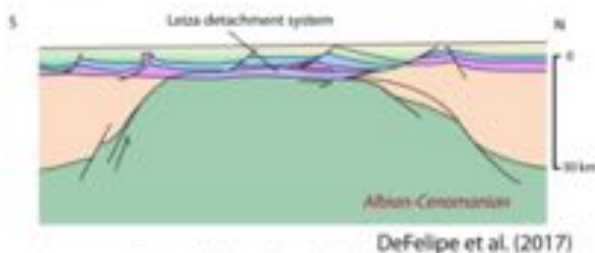
e. Central North Pyrenean Zone



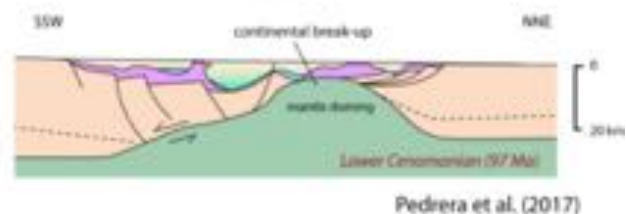
h. Eastern North Pyrenean Zone



f. Basque-Cantabrian basin (1)



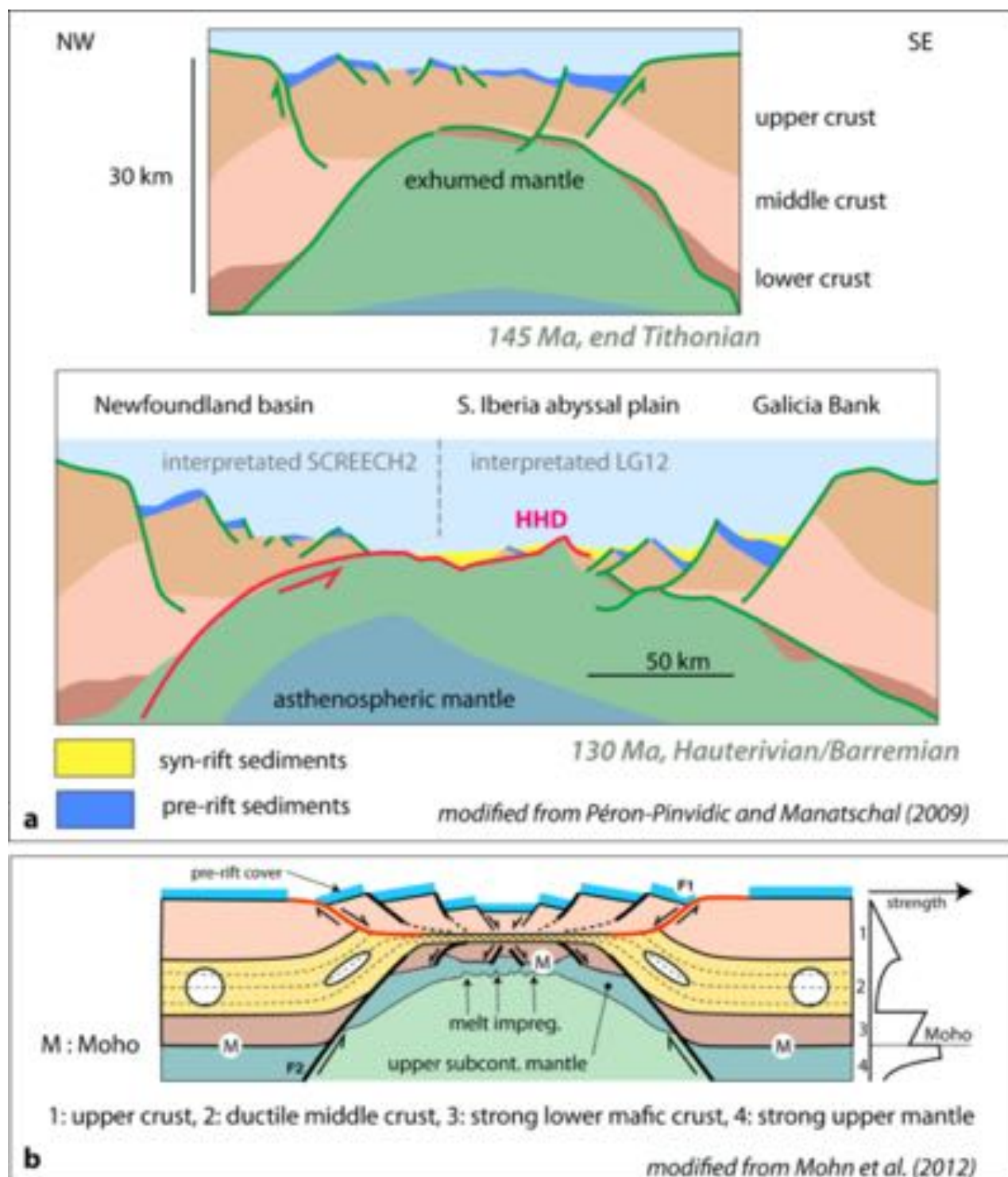
g. Basque-Cantabrian basin (2)



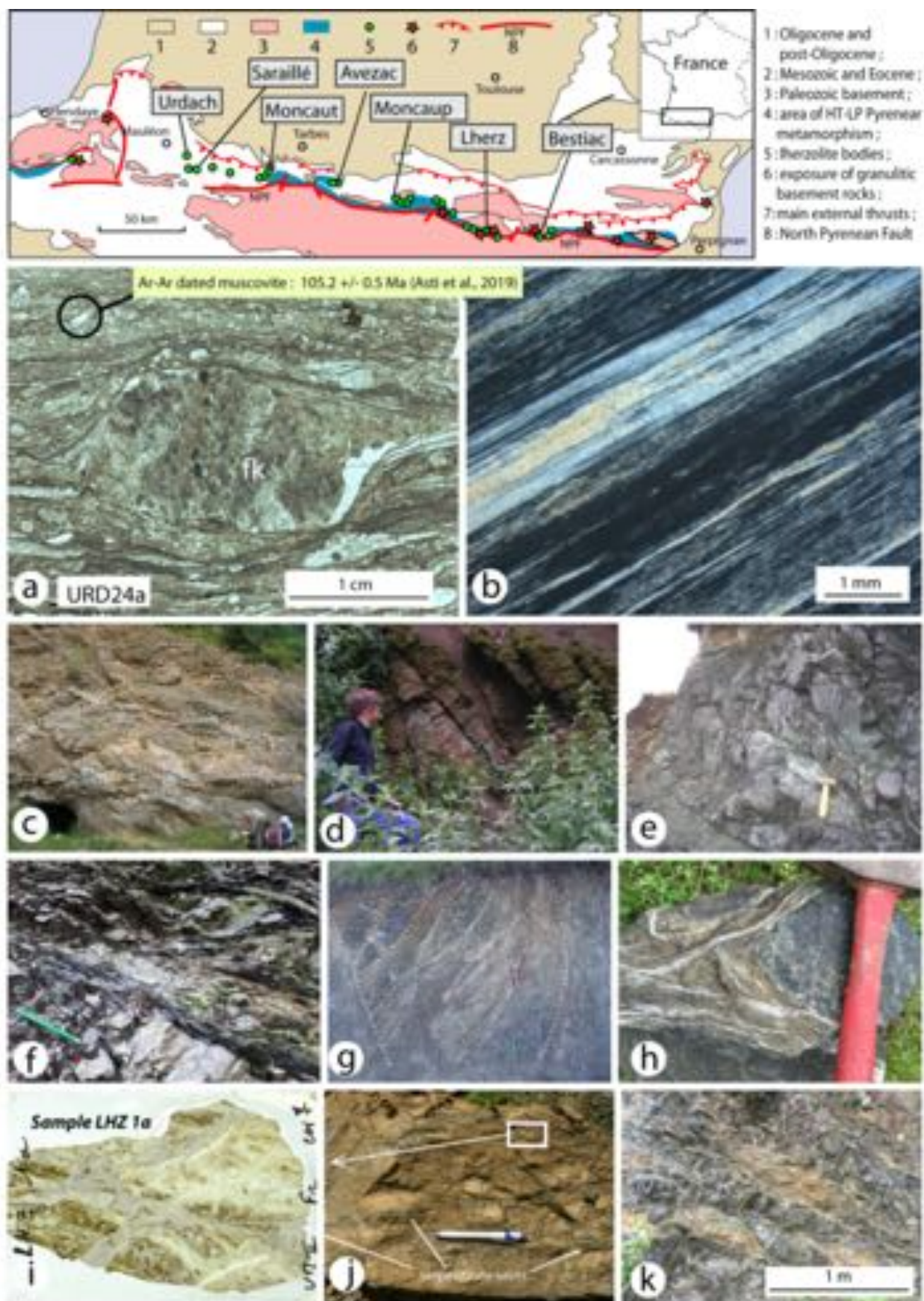
h. Basque-Cantabrian basin (3)



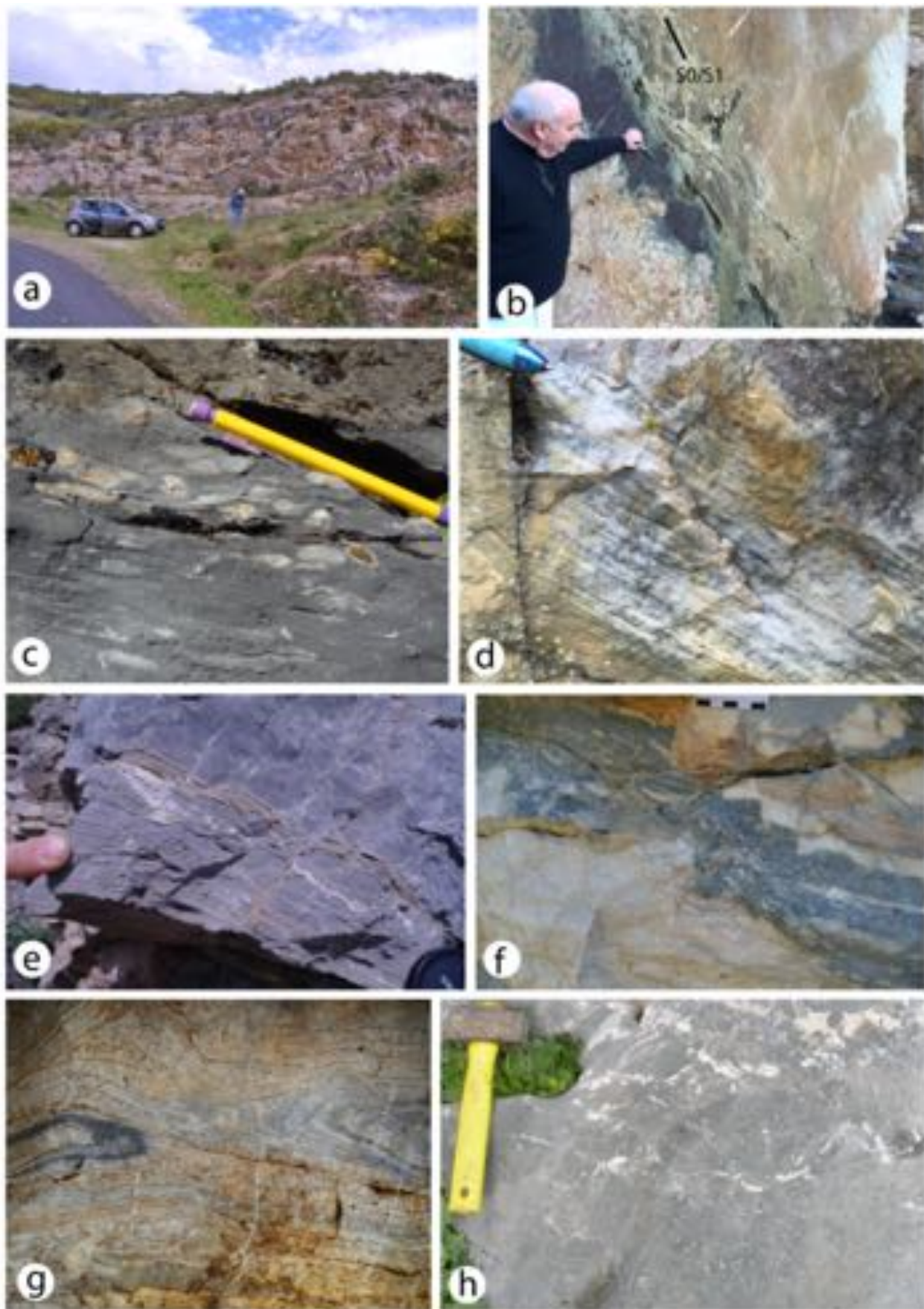
Lagabrielle et al., fig. 2, ESR, submitted



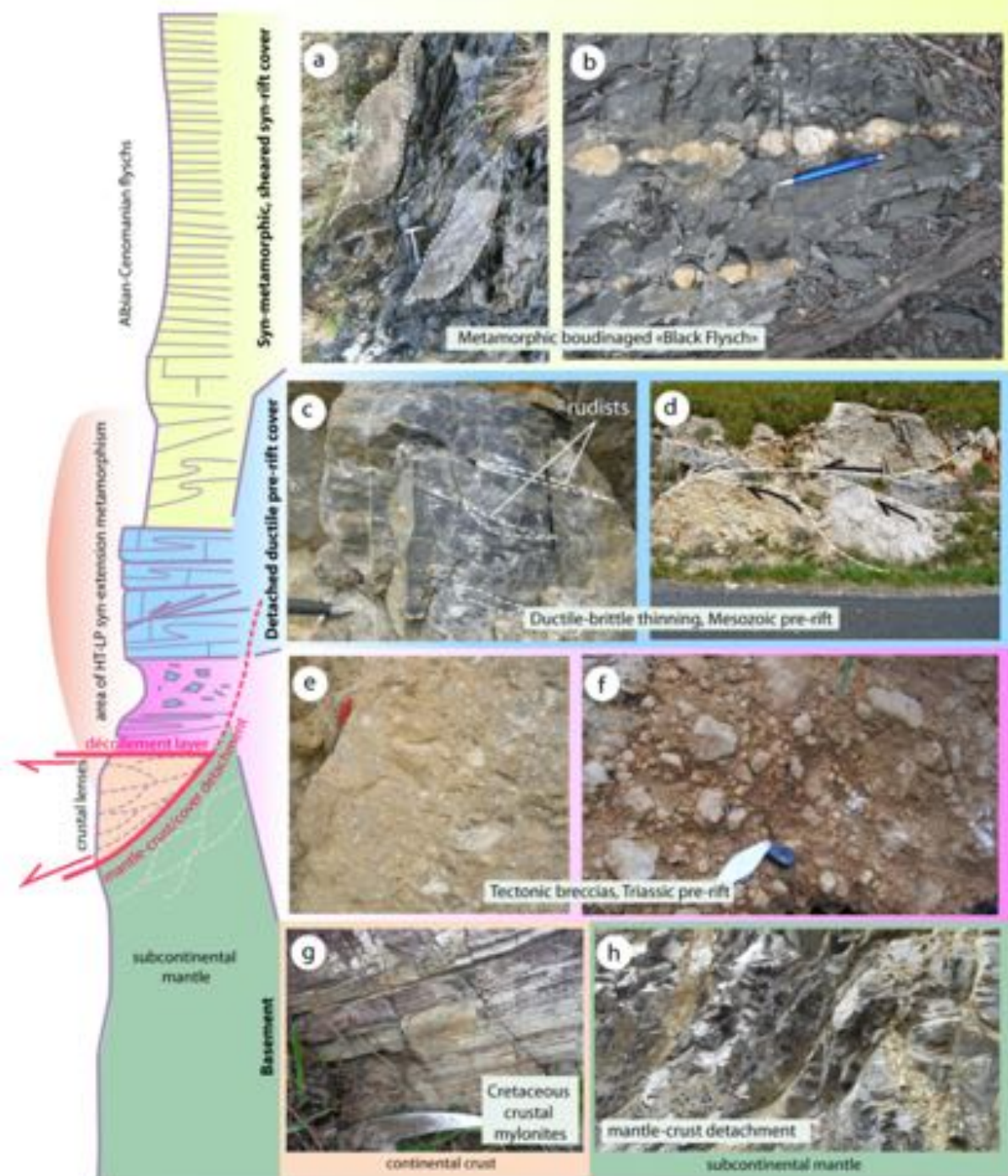
Lagabrielle et al., fig. 3, ESR, submitted



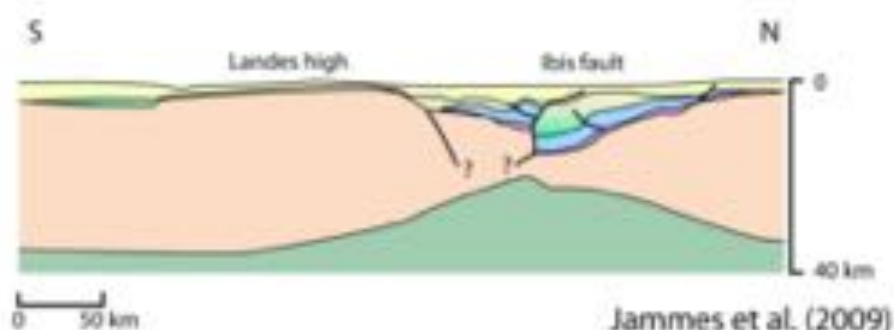
Lagabrielle et al., fig. 4, ESR, submitted



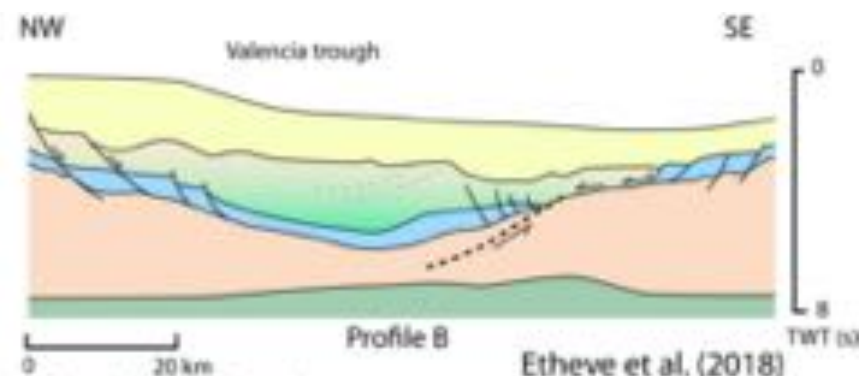
Lagabrielle et al., fig. 5, ESR, submitted



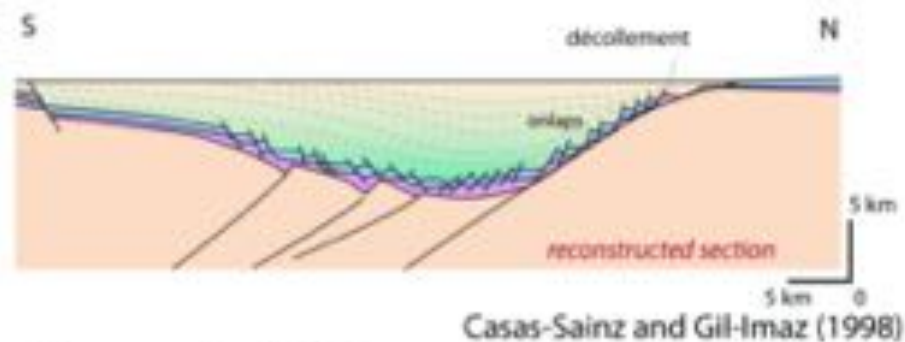
Lagabrielle et al., fig. 6, ESR, submitted



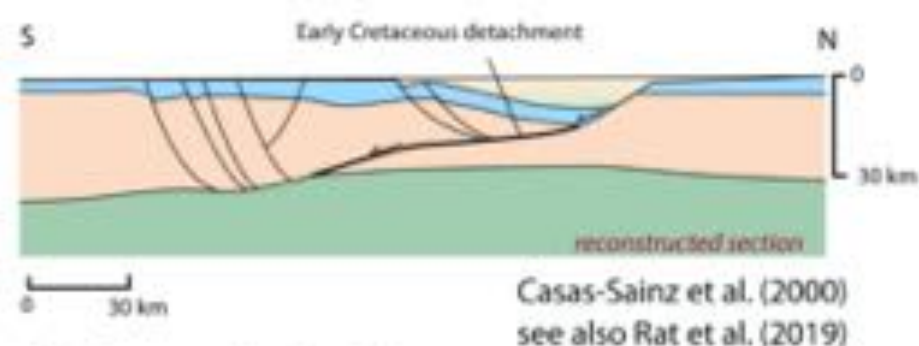
a. Parentis basin



b. Columbrets basin

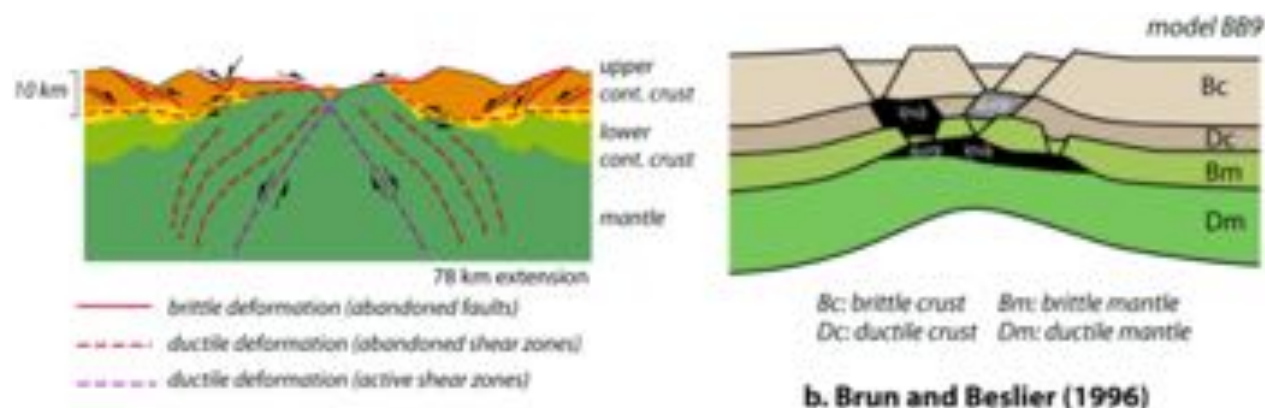


c. Cameros basin (1)



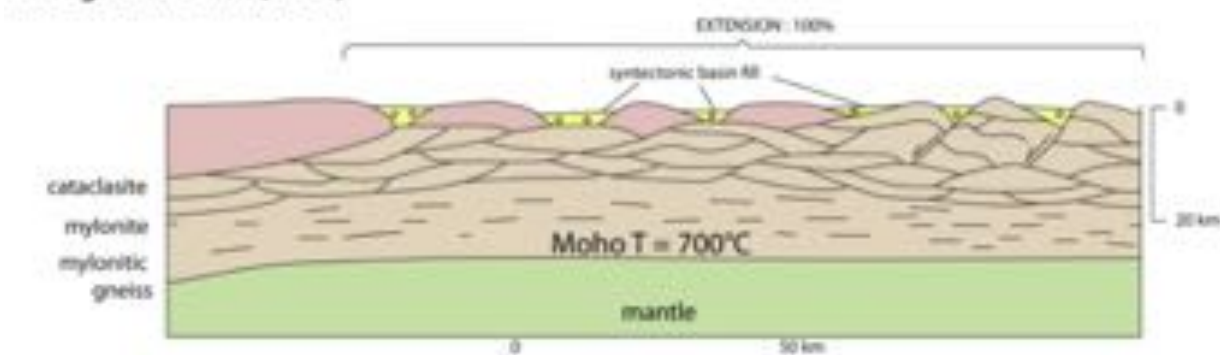
d. Cameros basin (2)



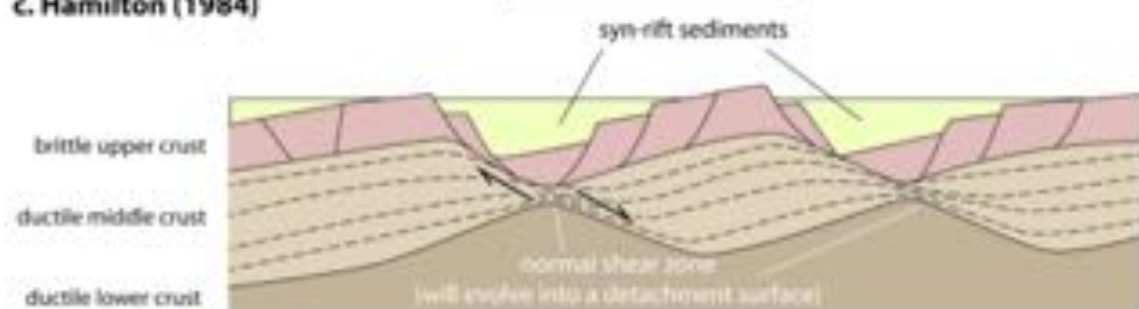


a. Nagel and Buck (2004)

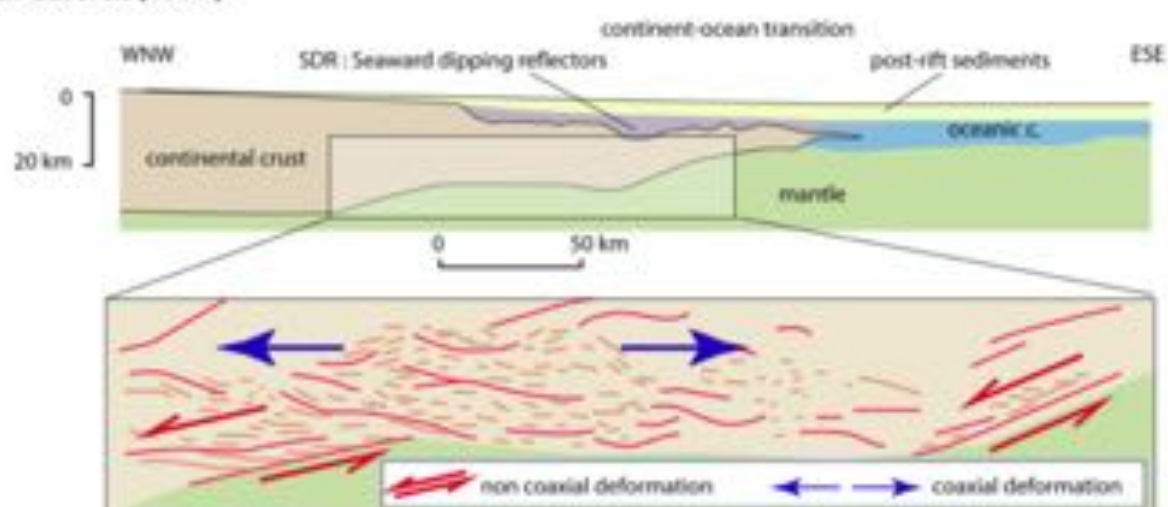
b. Brun and Beslier (1996)



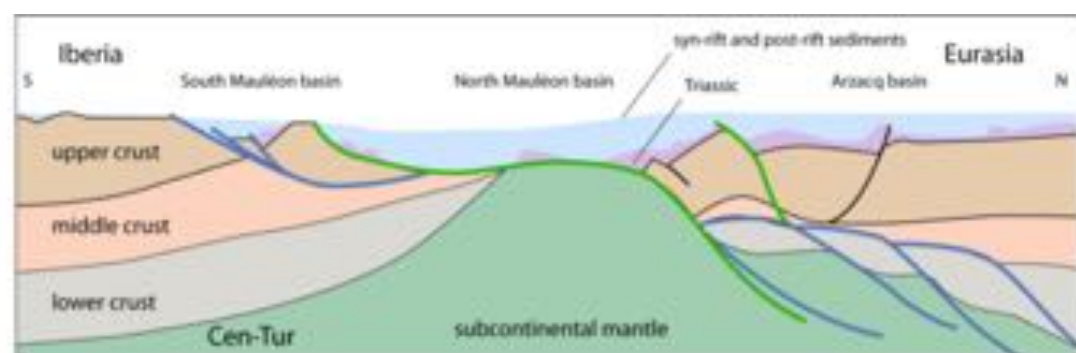
c. Hamilton (1984)



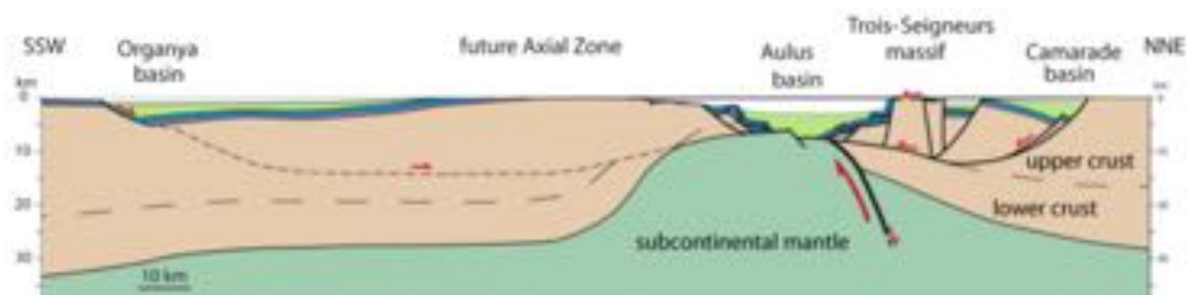
d. Gartrell (1997)



e. Clerc et al. (2018)



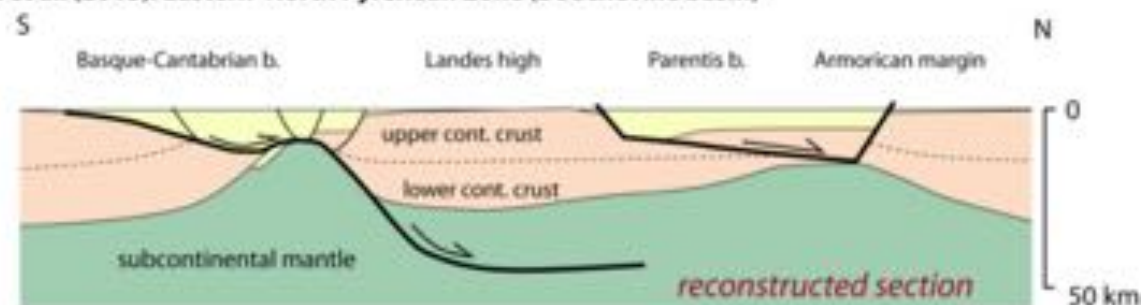
a. Masini et al. (2014): Mauléon basin



b. Lagabrielle et al. (2010): Central North Pyrenean Zone (Aulus basin, Etang de Lers)



c. Vauchez et al. (2013): Eastern North Pyrenean Zone (Boucheville basin)



d. Roca et al. (2011) : Basque-Parentis transect

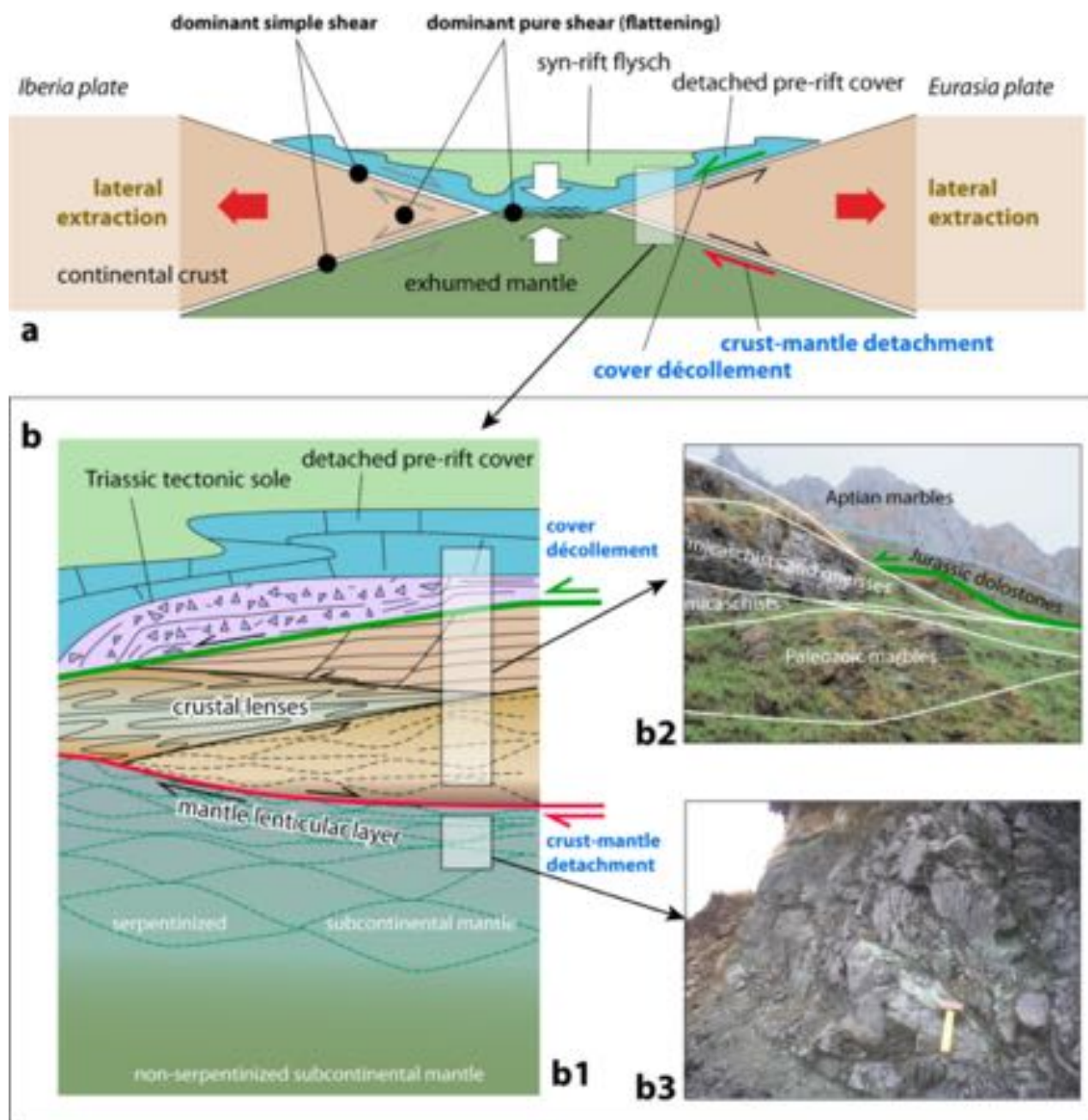
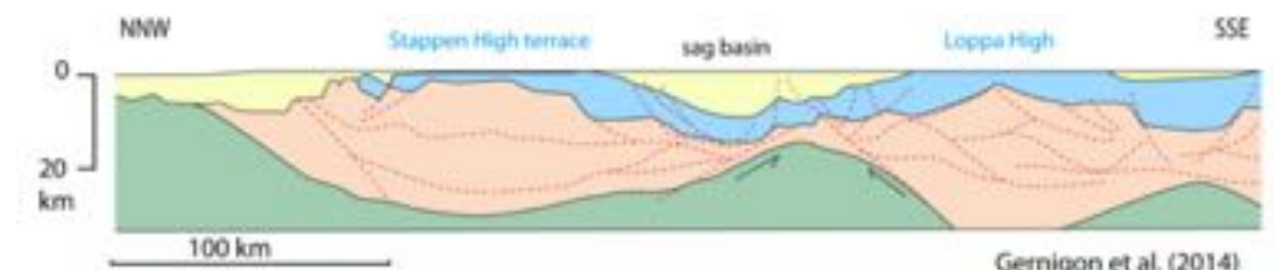


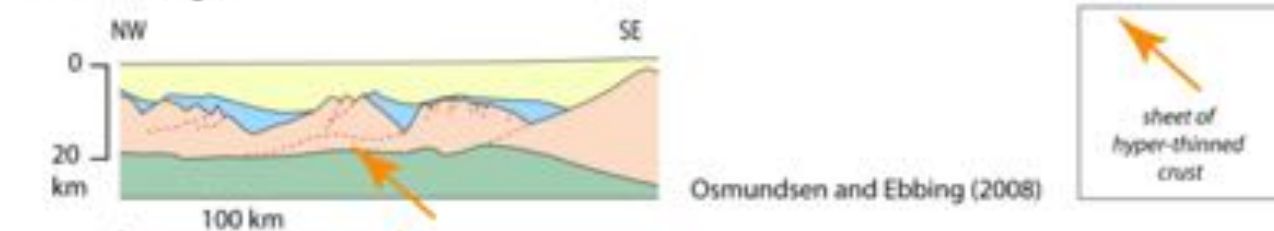
fig. 10

Lagabrielle et al., smooth slopes basins, submitted



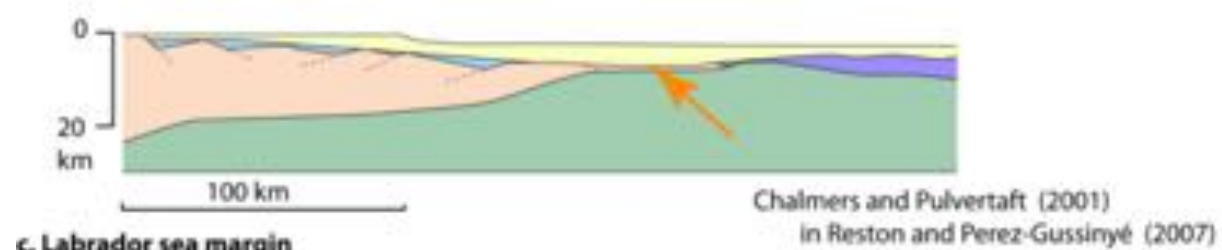
Gernigon et al. (2014)

a. Barents margin



Osmundsen and Ebbing (2008)

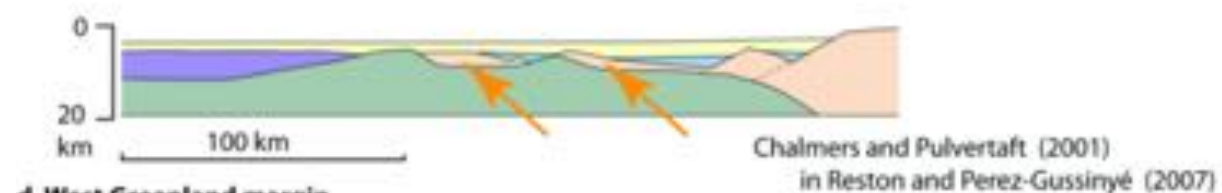
b. Northern More basin, Norway margin



Chalmers and Pulvertaft (2001)

in Reston and Perez-Gussinyé (2007)

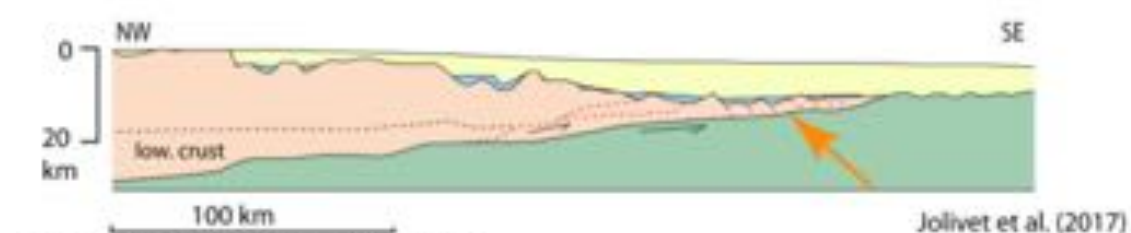
c. Labrador sea margin



Chalmers and Pulvertaft (2001)

in Reston and Perez-Gussinyé (2007)

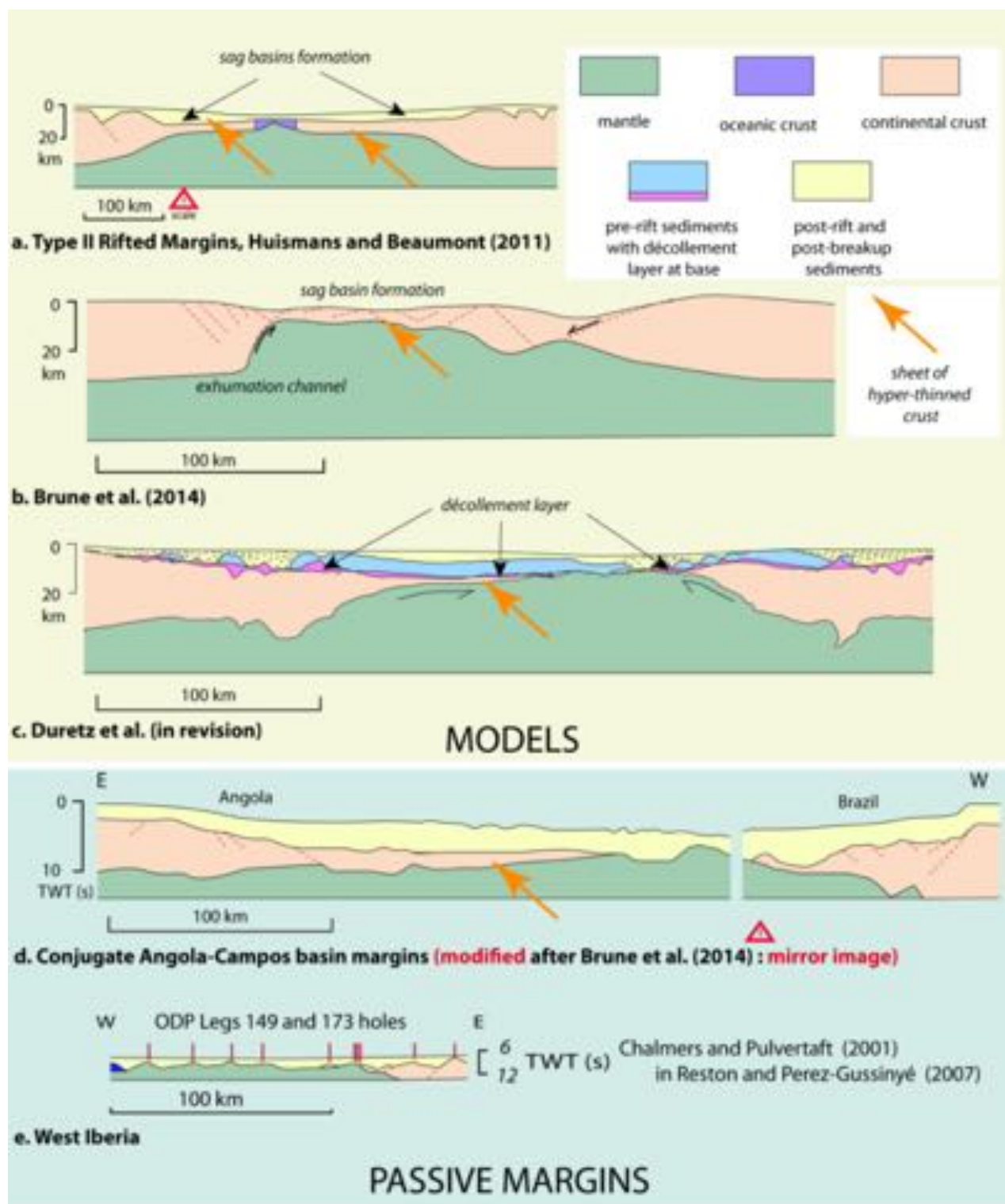
d. West Greenland margin

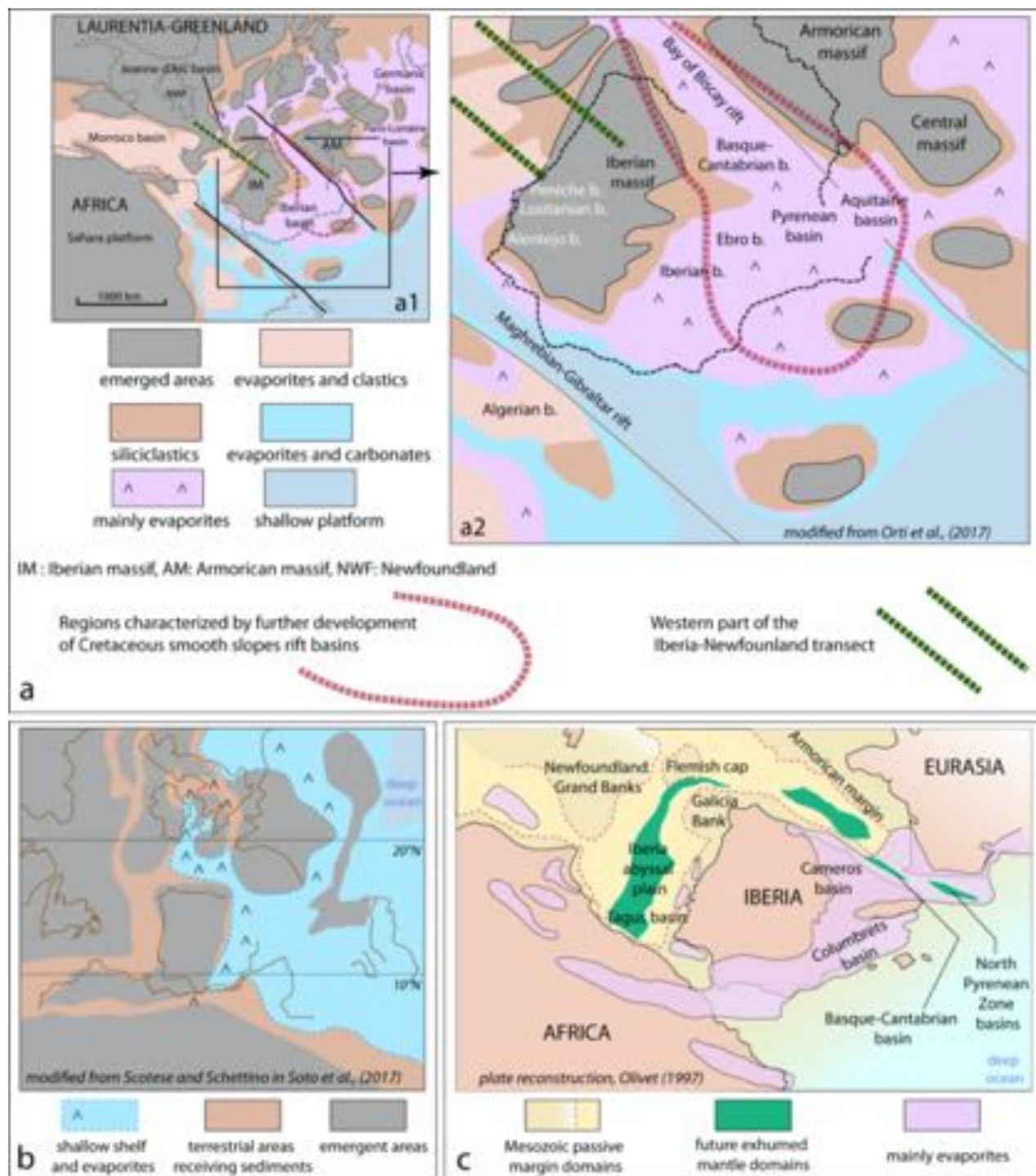


Jolivet et al. (2017)

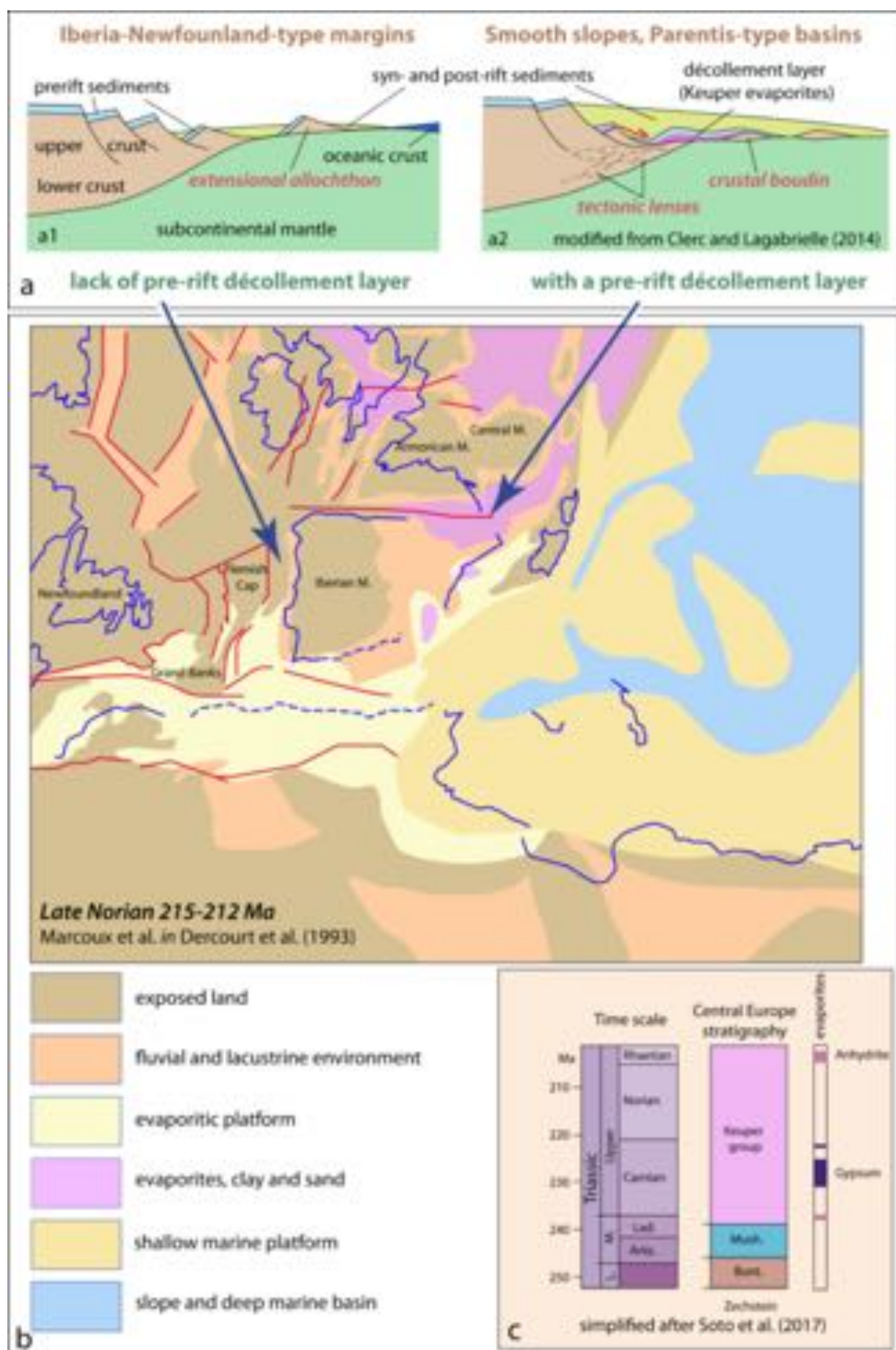
e. Western Mediterranean, Gulf of Lion

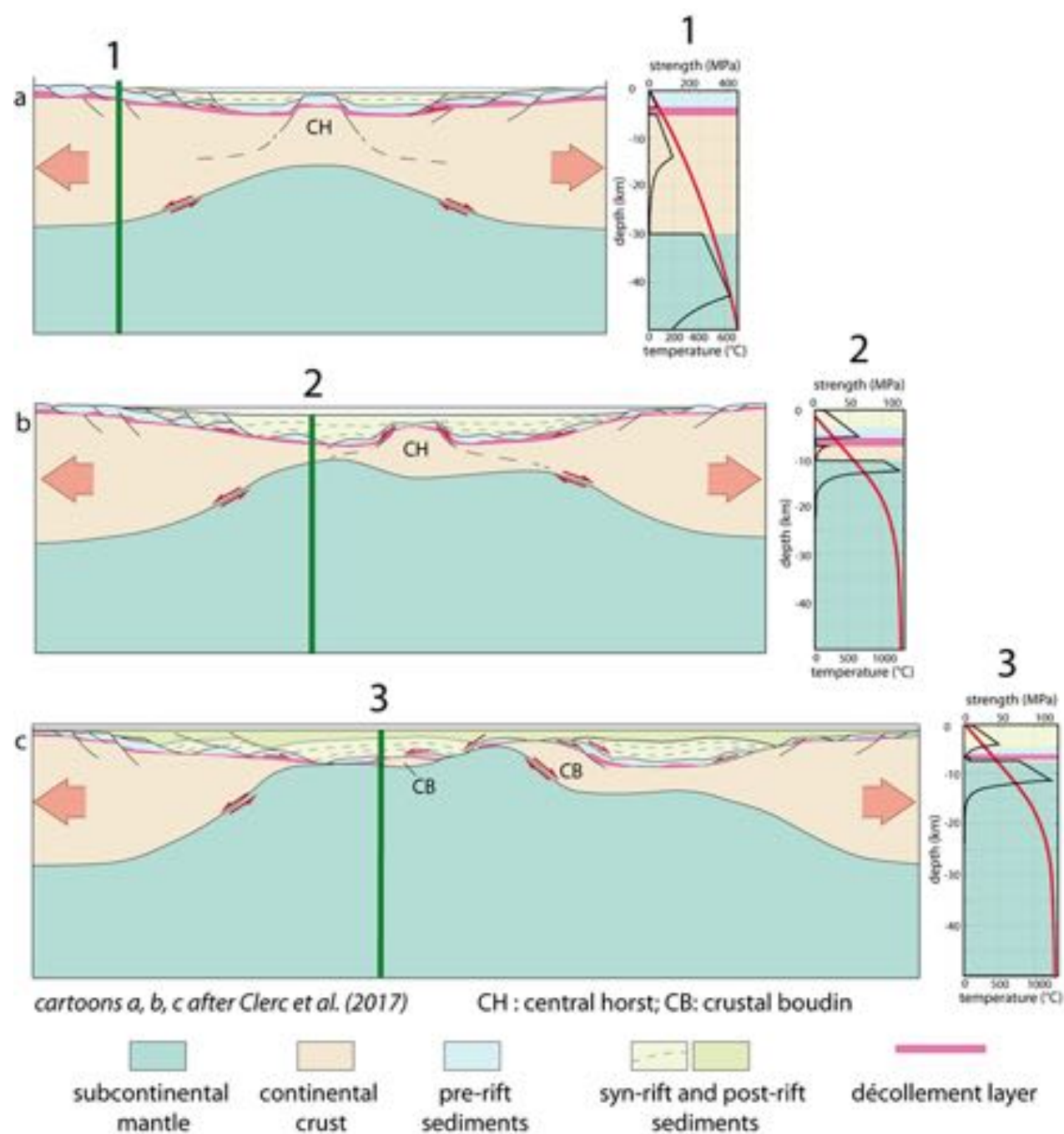




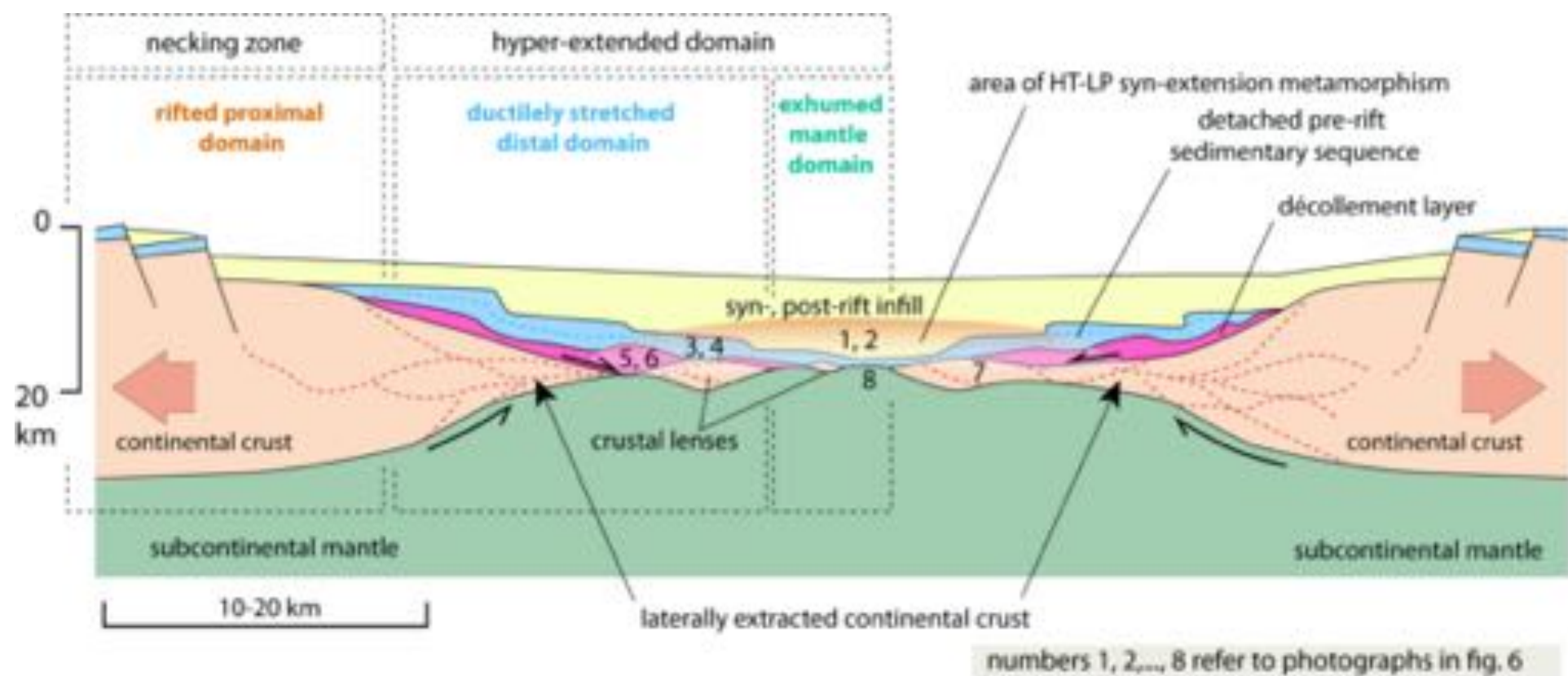


Lagabriele et al., fig. 13, ESR, submitted





Lagabrielle et al., fig. 15, ESR, submitted



Lagabrielle et al., fig. 16, ESR, submitted